Bioactive Materials 55 (2026) 515–528

Contents lists available at ScienceDirect

Bioactive Materials

journal homepage: www.keaipublishing.com/en/journals/bioactive-materials

Dimensional memory in glioblastoma mechanics: Traction force analysis of cells cultured in 2D versus 3D collagen environments

Mishal Khan [a], Philipp Kollenz [a], Maret Fritzenschaft [a], Fereydoon Taheri [a], Federico Colombo [a], Johannes W. Blumberg [b,c], Luise Schlotterose [d], Ulrich Sebastian Schwarz [b,c], Aldo Leal-Egaña [a], Christine Selhuber-Unkel [a,*]

[a] Institute for Molecular Systems Engineering and Advanced Materials (IMSEAM), Heidelberg University, Im Neuenheimer Feld 225, D-69120, Heidelberg, Germany
[b] BioQuant, Heidelberg University, Im Neuenheimer Feld 267, 69120, Heidelberg, Germany
[c] Institute for Theoretical Physics, Heidelberg University, Philosophenweg 19, 69120, Heidelberg, Germany
[d] Department of Anatomy, Kiel University, Otto-Hahn-Platz 8, 24118, Kiel, Germany

ARTICLE INFO

Keywords:
Glioblastoma mechanics
2D v/s 3D culture
3D collagen substrate
Dimensional memory
Traction force microscopy

ABSTRACT

Glioblastoma (GB) is one of the most aggressive and lethal brain tumors, characterized by rapid proliferation, diffuse infiltrative growth, therapeutic resistance, and molecular heterogeneity. A major challenge in studying GB is the lack of *in vitro* models that accurately replicate the tumor's cellular characteristics observed *in vivo*, particularly the importance of three-dimensional (3D) models. This study investigated the traction stress exerted by LN229 and T98G human GB cell lines, as well as the HMC3 human microglia cell line, using traction force microscopy. First, cells were cultured on two-dimensional (2D) collagen-coated surfaces and within three-dimensional (3D) collagen-based bioactive matrices. Afterward, these cells were extracted and reseeded on flat polyacrylamide gels coated with collagen type I to perform traction force microscopy, thereby directly probing the mechanical memory imparted by their prior 2D or 3D environments. Our findings reveal that GB cells exert substantially higher traction stresses when cultured on 2D collagen-coated surfaces compared to those cultured in 3D bioactive matrices. This underscores the relevance of protein-based bioactive materials, such as collagen scaffolds, in replicating *in vivo* tumor microenvironments to study GB behavior. Single-cell nano-indentation and focal adhesions quantification were performed to offer mechanistic insights into glioblastoma and microglia cells. Interestingly, in addition to notable differences in traction stresses between cells cultured in 2D and 3D collagen environments, glioblastoma showed significant variation based on the cell type in terms of single-cell stiffness and focal adhesion metrics. These findings underscore the importance of complementary biophysical assays and realistic 3D bioactive matrices when studying GB mechanics *in vitro*.

1. Introduction

Glioblastoma (GB), classified as grade IV astrocytoma, is the most aggressive and lethal primary brain tumor. It has a desolate prognosis, with a median survival typically under 15 months despite various treatment strategies like surgery, radiation, and chemotherapy [1,2]. Its high recurrence rate (~90 %) underscores the need for better therapies and reliable preclinical models [3].

While glioblastoma has long been studied from a molecular and genetic perspective, increasing attention has turned to its tumor microenvironment (TME), including mechanical and structural cues. The TME plays a pivotal role in glioma progression, resistance, and invasion [4–6]. GB cells interact dynamically with both cellular and acellular components of their microenvironment, sensing mechanical cues and responding through cytoskeletal remodeling, force generation, and changes in morphology [7–9]. A key player in this interaction is the

Peer review under the responsibility of editorial board of Bioactive Materials.
* Corresponding author.
E-mail addresses: khanmishal798@gmail.com (M. Khan), Philipp.kollenz@pci.uni-heidelberg.de (P. Kollenz), fritzenschaft.maret@gmail.com (M. Fritzenschaft), f.taheri@imseam.uni-heidelberg.de (F. Taheri), federico.colombo@imseam.uni-heidelberg.de (F. Colombo), johannes.blumberg@bioquant.uni-heidelberg.de (J.W. Blumberg), luise.schlotterose@dpag.ox.ac.uk (L. Schlotterose), schwarz@thphys.uni-heidelberg.de (U.S. Schwarz), aldo.leal.egana@bio-nanotech.org (A. Leal-Egaña), selhuber@uni-heidelberg.de (C. Selhuber-Unkel).

https://doi.org/10.1016/j.bioactmat.2025.09.025
Received 31 March 2025; Received in revised form 31 July 2025; Accepted 16 September 2025

extracellular matrix (ECM), which does not merely provide structural support but actively shapes tumor behavior [10] and also controls the effect of mechanical cues on cell responses [11]. In GB, ECM components such as collagen, fibronectin, laminins, and hyaluronic acid influence cell adhesion, migration, and invasion [12–15]. Adhesion sites, nutrient gradients, and biochemical signals contribute to dynamic structural remodeling, further reinforcing GB's highly invasive phenotype [4]. The ECM also responds to mechanical forces exerted by tumor cells, creating a feedback loop that promotes malignancy [15,16].

Indeed, biomechanical characteristics, such as the ability of cells to generate and respond to traction forces, have emerged as hallmarks of malignancy and cancer progression. Unlike many solid tumors that metastasize via the bloodstream, GB infiltrates diffusely into surrounding brain tissue. This invasion is tightly linked to how tumor cells interact with and deform the ECM [17–19]. Understanding these cell-matrix mechanical interactions is therefore critical to grasping the invasive potential of glioma cells.

However, dissecting these mechanobiological processes *in vitro* presents its own challenges. Traditional GB research has relied extensively on *in vivo* systems [20] and two-dimensional (2D) cell culture systems. While *in vivo* models (particularly rodents) provide biological context, they often suffer from interspecies differences that limit clinical translation [21]. Conversely, culturing cells on 2D surfaces allows for highly controlled experiments but lacks the mechanical and topographical complexity of the brain's native 3D microenvironment [22]. Cells grown on rigid 2D plastic surfaces adopt flattened morphologies and exhibit altered gene expression, cytoskeletal organization, and signaling activity compared to 3D environments [22–24]. These limitations have prompted a shift toward 3D biomimetic culture systems, which better replicate *in vivo*-like conditions [3,25–27].

Among ECM components, Collagen type I is extensively utilized in 2D and 3D GB models due to its tunable mechanical properties and biological relevance [24,28–31]. By modulating collagen concentration or enzymatic cross-linking, researchers can mimic different stiffness levels of brain tissues [32,33]. Studies show that GB cells exhibit enhanced cellular mobility in low-concentration collagen hydrogels (3–5mg/mL) compared to high-concentration hydrogels (10 mg/mL), making these models physiologically relevant for investigating the mechanics of invasion [28,31].

Building on collagen-based 2D and 3D culture models, it is essential to assess how prior dimensional context influences the biomechanical behavior of glioblastoma cells. To do so, we employed traction force microscopy (TFM), a widely used technique to quantify cell-generated forces by tracking bead displacements on compliant, ECM-coated polyacrylamide gels [34–38]. These gels are well-established as linearly elastic over physiologically relevant strains and geometrically linear within the small deformations imposed during TFM, justifying the use of linear elasticity assumptions in force calculations. Importantly, the linear elastic properties of the substrate are material-dependent and remain valid irrespective of the cell type cultured [39–41].

While TFM has been widely applied in models of breast, lung, and prostate cancers [42–44], its application in glioblastoma (GB) remains limited. TFM has been applied to study cell-matrix interactions in both 2D and 3D environments [34,36,45–47]. To our knowledge, there are no published studies investigating how prior culture conditions—specifically, 2D versus 3D collagen microenvironments imprint a mechanical phenotype on GB cells that persists when the cells are subsequently reseeded on identical 2D substrates. This approach bridges the gap between dimensional culture history and dynamic cell mechanics in glioblastoma, revealing the impact of mechanical memory.

It is now well established that the dimensional context in which cells are cultured influences their morphology, cytoskeletal organization, and force-generating behavior, as shown in studies of cellular mechanical memory [48]. Cells preconditioned in 3D matrices exhibit different cytoskeletal organization and force-generating capacities compared to 2D-cultured counterparts, as demonstrated in recent studies using TFM in cancer models [49,50]. However, such effects have not been systematically explored in GB, particularly in relation to non-malignant CNS cell types.

While astrocytes and neural progenitors are often considered the putative cells of origin in glioblastoma, we selected microglia (HMC3) as a comparator because they are the predominant non-malignant, CNS-resident cell type within the GB tumor microenvironment. Microglia are resident immune cells that are highly interactive with tumor cells, actively shaping tumor progression through chemotactic signaling, extracellular matrix remodeling, and physical interactions. Importantly, like astrocytes and neural stem cells, microglia are not transformed cells in their natural state. However, their abundance and dynamic role in the tumor microenvironment make them a biologically and mechanically relevant reference for distinguishing glioblastoma-specific force profiles from those of other CNS-resident cells. This rationale supports their inclusion as a non-malignant comparator in our study [51–56].

To address this, we characterized the traction stress exerted by two GB cell lines (LN229 and T98G) and compared them with that of the non-malignant human microglia cell line HMC3. To investigate the impact of dimensionality, cells were cultured on collagen type-I-based 2D hard substrates and within 3D soft bioactive substrates. We aimed to assess whether dimensional memory persists in GB and microglia cells and to evaluate the physiological relevance of this phenomenon using a well-defined *in vitro* traction force assay, complemented by quantitative analyses of focal adhesions and cellular stiffness.

2. Results and discussion

We began by characterizing the biomechanical profiles of two glioblastoma cell lines, LN229 and T98G, and the non-malignant HMC3 microglia, following pre-culture in either a hard 2D or a soft 3D collagen environment (Fig. 1). LN229, a highly tumorigenic line with epithelial-like characteristics [57,58] and T98G, a less tumorigenic, mesenchymal-like line [59,60]provided contrasting models to assess dimensional memory in malignant cells. By comparing force generation, focal adhesion organization, and cortical stiffness after reseeding on standardized 2D substrates, we aimed to determine whether pre-culture conditioning in different dimensional environments leaves a lasting mechanical imprint.

We first performed a proliferation assay to determine whether the composition of the collagen type-I-based substrates affects the biological activity of HMC3, LN229, or T98G. This study involved cells seeded on 6-well plates coated with collagen type-I (2D), collagen type-I-based bioactive matrices (3D), and conventional cell culture flasks (control). As shown in Fig. 2, all cell lines maintained their proliferative capacity across all three conditions, indicating that collagen-based substrates did not impair their biological activity. However, the assays revealed distinct differences in proliferation dynamics among the cell lines.

HMC3 microglial cells showed similar proliferation trends under control and 2D conditions, which may indicate that surface coating with collagen did not substantially affect their growth. In contrast, HMC3 cells in 3D collagen matrices exhibited slower proliferation and longer duplication times, indicating that the dimensionality of the matrix impacts their proliferative capacity more than substrate composition alone [62]. LN229 glioblastoma cells exhibited comparable overall proliferation rates across all three conditions. However, their duplication time was shorter in 3D matrices than in 2D or control conditions, indicating a subtle effect of matrix dimensionality on their duplication time [24] Whereas, T98G glioblastoma cells demonstrated faster proliferation in 2D collagen conditions than in the control. Compared to the 3D matrix, the 2D and control conditions supported a higher proliferation rate, and a clear difference in duplication time was observed between 2D and 3D environments [29].

In addition to assessing cell proliferation, this assay was used to determine the optimal day of cell confluence for each condition and cell line. These time points were used as reference for extracting cells from

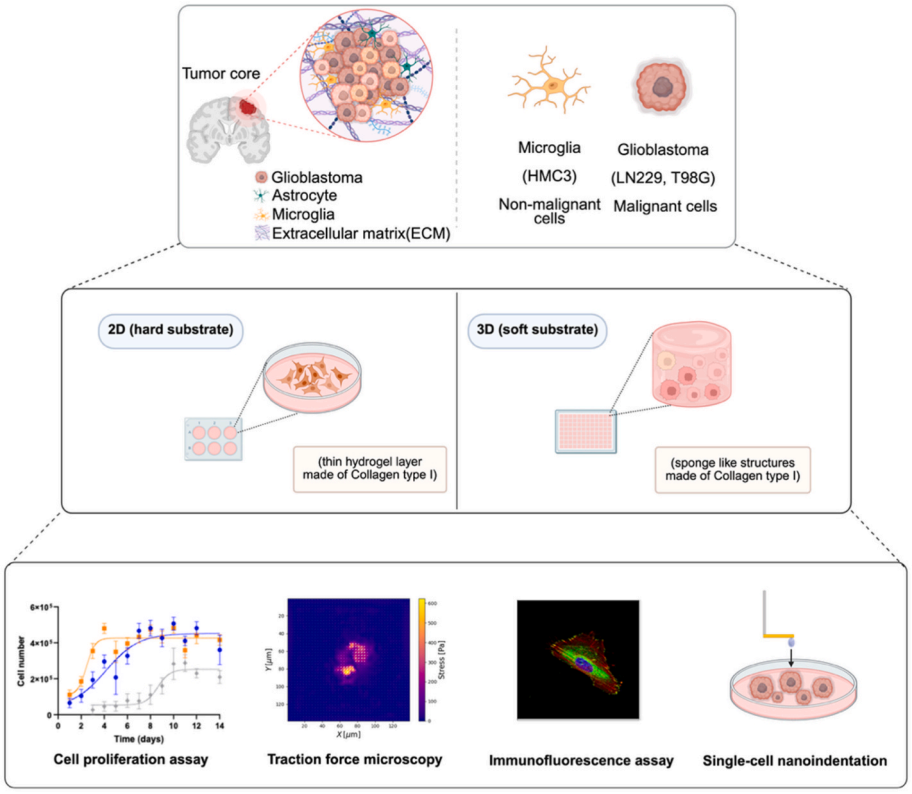

Fig. 1. A schematic of experimental design including representation of GB tumor microenvironment where glioblastoma cells also interact with other cell types, i.e., microglia and astrocytes, etc. This research includes glioblastoma cell lines (T98G and LN229) and microglia cell line HMC3, which were set in two pre-culture conditions, i.e., 2D and 3D, to perform a cell proliferation assay further followed by single-cell traction force microscopy, immunofluorescence assays, and single-cell nanoindentation studies [61].

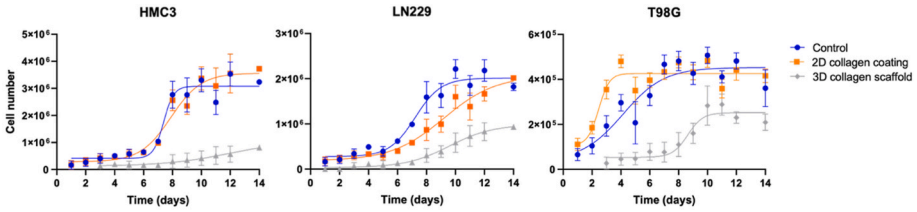

Fig. 2. Representative graphs of the cell proliferation assay of HMC3, LN229, and T98G. In these graphics, the gray curve represents the duplication of cells in the 3D condition, while the orange and blue curves depict the proliferation of cells under 2D conditions and control, respectively.

their respective pre-culture conditioning environments (2D, 3D, or control) for reseeding on 2D surfaces, i.e., collagen-coated polyacrylamide gels, glass cover slips, and plastic well plates. The reseeded cells were then analyzed in downstream experiments, including traction force microscopy (TFM), focal adhesion characterization, and nanoindentation measurements (Fig. 1). The 3D cultures were kept sufficiently thin (~400 μm) and low in collagen density (~3.5 mg/ml) to minimize nutrient diffusion limitations and avoid hypoxia-induced artifacts [24,28–31].

Traction force microscopy (TFM) was performed using collagen type-I functionalized polyacrylamide (PAA) hydrogels embedded with fluorescent microbeads [39,64] (as illustrated in Fig. 3A). PAA hydrogels are widely used for TFM due to their optical transparency, mechanical tunability, and inherent homogeneity, which allow for precise measurements of cell-generated forces [65,66]. To verify that our PAA hydrogels provided a representative and uniform mechanical environment for single-cell TFM measurements, matrix scan-based nanoindentation was performed across multiple regions of each polyacrylamide gel to assess relative homogeneity and reproducibility of mechanical properties [67,68]. Across n = 112 measurement points sampled from three independently prepared gels (see Supplementary Fig. S1; Table S1), nanoindentation revealed a mean Young's modulus of 3.64 ± 0.37 kPa (Fig. 2B, one representative gel). Our measured mean stiffness was approximately 17 % higher than the target value (3.13 ± 0.42 kPa), which is well within the typical 10–20 % variability reported for polyacrylamide gels prepared by hand [64].

The mean Young's modulus exhibited a coefficient of variation (CV) of 10.72 % across all the samples (see Supplementary Fig. S1; Table S1), indicating good spatial uniformity. This falls within the upper end of the 5–10 % range typically reported for polyacrylamide gels of similar stiffness and remains well below the generally accepted threshold (<15 %) for hydrogel characterization in cell mechanics studies. Such variability is consistent with published standards, particularly when accounting for minor batch-to-batch differences and the effects of overnight PBS storage [40,41,69,70].

In addition to mapping stiffness, our nanoindentation protocol (see Supplementary Information Section 1) directly confirms both material and geometrical linearity required for Hertzian analysis. Moreover, all

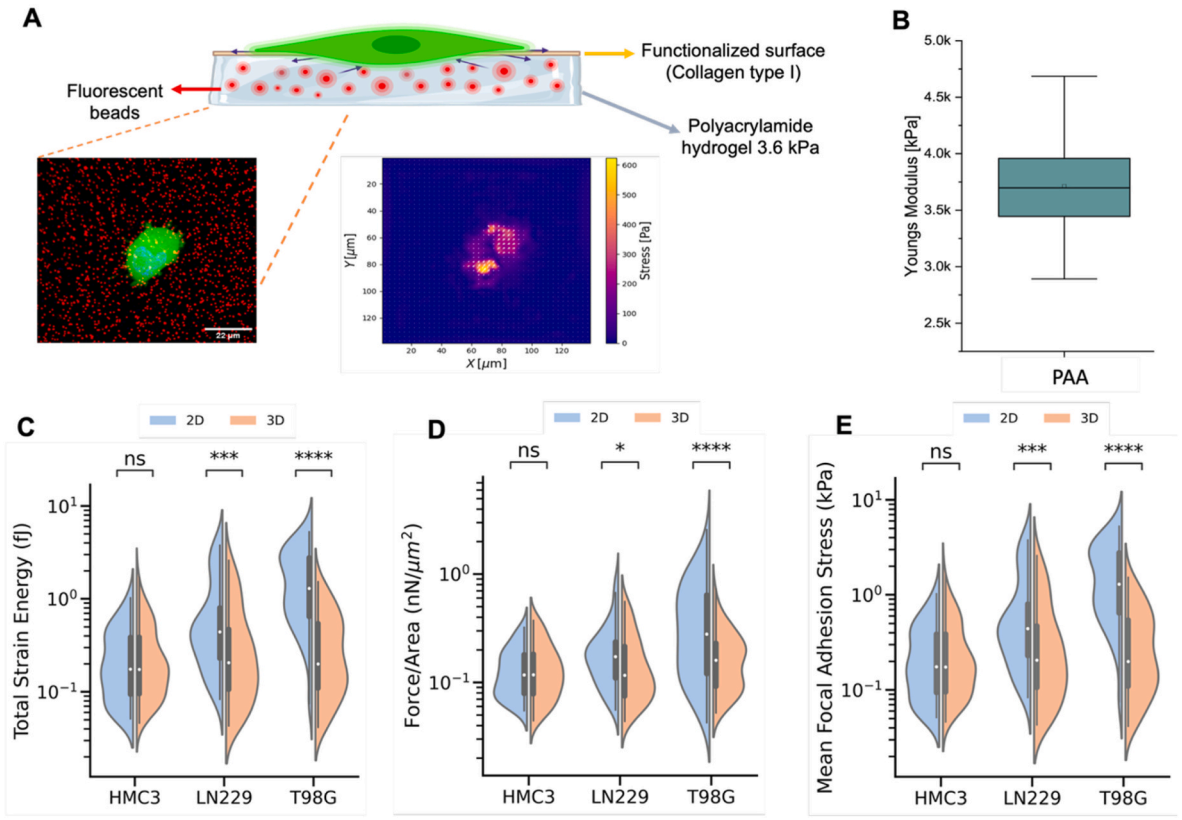

Fig. 3. (A) Illustration of the method to analyze traction stress exerted by single cells [63]. This analytical strategy requires a flat polyacrylamide hydrogel functionalized with collagen type I. (B) The box plot represents the elastic properties of the aforenamed PAA hydrogel from one representative gel of three independently prepared PAA gels; data from all three gels are shown in Supplementary Fig. S1, measured by nanoindentation, exhibiting an average elasticity of approximately 3.6 kPa (measured as Young's modulus). (C) Quantification of the total strain energy exerted by single cells after being extracted from 2D hard substrates and 3D soft substrates, later anchored to polyacrylamide hydrogels functionalized with collagen type I. (D) Determination of the F/A ratio for HMC3, LN229, and T98G. (E) Mean focal adhesion stress for each cell line in both culture conditions. Data represent pooled measurements from 5 to 10 independent experiments per condition, (n = 85–193) cells per condition. Mann-Whitney *U* Test was performed after random resampling for statistical analysis between two conditions for (C), (D), and (E), where *p < 0.05, ***p < 0.001, and ****p < 0.0001.

load–indentation curves (Supplementary Fig. S1B) fit the Hertz model with $R^2 \geq 0.95$, and display minimal hysteresis, demonstrating an essentially linear elastic response [71–73]. These results validate our assumption of a constant Young's modulus and support the accuracy of our substrate mechanics for subsequent TFM calculations. However, while nanoindentation provides valuable microscale mechanical characterization data [74–76], it should be regarded as complementary rather than definitive for validating TFM substrate assumptions. It confirms that the substrate behaves as a homogeneous, linear elastic material, thereby underpinning the reliability of our traction-force measurements [76–78].

Based on this mechanical validation, TFM experiments were performed to quantify how cellular forces deform the polyacrylamide substrate embedded with fluorescent microbeads. These bead displacements in the X/Y plane were tracked by confocal microscopy and converted into traction stresses based on the computational analysis [36,79,80] as illustrated in Fig. 3A. The mechanical work performed by HMC3, LN229, and T98G cells to deform the substrate, quantified as total strain energy following pre-culture in 2D or 3D collagen environments, is summarized in Fig. 3C and Table 1.

Notably, glioblastoma cells retained distinct biomechanical phenotypes even after being reseeded onto 2D TFM substrates. Specifically, LN229 and T98G cells, which were previously cultured in 3D, exerted significantly lower traction stress and total strain energy compared to their 2D-cultured counterparts (Fig. 3C–E & Table 1), consistent with a mechanical memory effect similar to that described in human stem cells [81]. These differences can be attributed to both the microenvironmental context experienced during pre-culture conditioning and the inherent cellular characteristics of glioblastoma and microglia cells.

Table 1
Quantitative traction force microscopy measurements: total strain energy, traction stress (force per area, F/A), and mean focal adhesion (FA) stress. Data are presented as n = X cells per condition from Y independent experiments. Statistical comparisons were performed using the nonparametric Mann–Whitney *U* test.

Cell	Culture	X	Y	Total Strain Energy (fJ)	Force/Area (nN/um^2)	Mean FA stress (kPa)
HMC3	2D	85	5	0.74 ± 0.11	0.14 ± 0.01	0.27 ± 0.03
HMC3	3D	90	6	0.37 ± 0.06	0.15 ± 0.01	0.29 ± 0.03
LN229	2D	137	9	2.01 ± 0.34	0.22 ± 0.02	0.87 ± 0.1
LN229	3D	158	9	0.73 ± 0.13	0.16 ± 0.01	0.36 ± 0.05
T98G	2D	193	10	17.9 ± 2.6	0.49 ± 0.05	2.16 ± 0.18
T98G	3D	153	9	0.86 ± 0.15	0.19 ± 0.01	0.38 ± 0.04

Glioblastoma cell lines (LN229 and T98G) demonstrated a significant difference in total strain energy when comparing microenvironmental changes experienced after 2D and 3D pre-culture conditions. It shows that cells that were precultured on 2D collagen surfaces and then reseeded on a flat polyacrylamide substrate typically spread out and form extensive focal adhesions [22], which exert strong, localized pulls on a stiff surface, generating higher total strain energy and traction stress. In contrast, 3D collagen bioactive matrices create a more physiologically relevant environment for the cells [82]. Depending on the

intrinsic properties of cells, they often adopt a more rounded or elongated morphology with fewer, more dynamic adhesions [28,29]. This altered organization, i.e., reduced cell-substrate coupling, usually results in lower total strain energy and overall traction stress.

LN229 exhibited a moderate difference in total strain energy as compared to T98G (Fig. 3C and Table 1). This may indicate differences in their invasive mechanisms. Studies show that LN229 cells tend to have a faster proliferation rate and weaker invasion ability, i.e., this type of glioblastoma cell likely relies on protease-dependent ECM degradation for invasion, thus requiring less mechanical work to deform the TFM substrate. [57,83–86]. In contrast, T98G cells appeared to be more invasive than LN229 [87,88]. This type of glioblastoma cells relies on mechanical force-dependent invasion [57,59,60], resulting in higher total strain energy as cells deform the TFM substrate.

However, since the magnitude of total force exerted by single cells is proportional to their spreading area (i.e. the larger the cells, the higher the magnitude of total forces) [89–91], the normalization of the forces exerted by anchored cells (relative to their surface) is essential to prevent misinterpretation of the experimental data, especially in case of heterogeneous cell populations exhibiting a wide range of biomechanical phenotypes [92,93]. This comparison can be made by determining the ratio of Force/Area (F/A) for traction stress (Fig. 3D & Table 1). The low traction stresses exerted by glioblastoma cells observed in our study are consistent with previously reported values for other glioblastoma cell lines, such as U87 and patient-derived cells, thereby validating our experimental setup and providing a benchmark for comparison [9,32,94,95]. However, to our knowledge, similar quantitative measurements have not been reported for LN229, T98G, or HMC3 cells, nor have previous studies systematically compared these cell types across 2D and 3D collagen environments using a combination of traction force microscopy, focal adhesion analysis, and single-cell stiffness measurements. This underscores the novelty of our work in extending the mechanobiological characterization of these specific cell lines to different dimensions. As illustrated in Fig. 3D, the ratio F/A of glioblastoma cells exhibits a distinctive difference among 2D and 3D culture conditions and among both glioblastoma cell lines.

These assays also reveal that both malignant cell types generate a wide range of traction stresses and strain energies, underscoring their mechanical heterogeneity. In this regard, it is important to mention that cellular heterogeneity, generated by mutations or chromosomal instability and other factors, is one of the mechanisms used by cancer cells to enhance their aggressiveness, becoming resistant to several treatments, such as chemotherapy or radiotherapy [1,92,96]. These findings highlight the distinct mechanical behaviors of glioblastoma cell subtypes and their adaptation to different microenvironmental conditions.

HMC3, a non-malignant microglia cell line, displayed no significant differences in total strain energy or traction stress between 2D and 3D pre-cultured conditions (Fig. 3C, D & Table 1). While 3D soft substrates do not compromise microglia cell viability, they can alter cell morphology [97,98], which may contribute to reduced traction stress. Microglia, including HMC3, typically remain in a resting state until activated by external signals to perform specific functions [56,99,100]. HMC3 is a non-malignant cell line with most likely no invasion profile, so its biomechanical activity is inherently lower, leading to reduced force generation unless activated by external stimuli (e.g., glioblastoma-secreted factors or inflammatory signals) [98].

The forces exerted at individual focal adhesions were analyzed to compare cells cultured on 2D and in 3D collagen environments. As shown in Fig. 3E and Table 1, the mean focal adhesion stress (determined by selecting visible focal adhesions from the traction stress map) follows the same trend as observed for total strain energy (Fig. 3C) and Force/Area (Fig. 3D). For each focal adhesion point, we calculated the mean stress within a (1.5 μm^2) surrounding area in both x and y directions and then took the absolute value by normalizing the x and y components. These forces are predominantly generated by mature focal adhesion (see Supplementary Fig. S2), which are characterized by a higher concentration of cytoskeleton and integrin proteins [101,102]. This quantification helps determine whether the exertion of biomechanical forces would be related to the increased activity of the actomyosin machinery (i.e., due to the magnitude of forces involved directly at the cell-matrix interface) or due to the density of focal adhesions located on the cell surface. Consistent with the total strain energy and traction stress data, HMC3, LN229, and T98G exhibit distinct mean focal adhesion stresses, underscoring the influence of both dimensionality and cell type on their mechanical behavior.

Next, to investigate the impact of prior culture dimensionality on cell morphology and adhesion, we performed immunostaining for F-actin, vinculin, and nuclei in HMC3 microglia and LN229 and T98G glioblastoma cells that were previously cultured in 2D or 3D collagen environments, as well as in cells maintained under conventional plastic (flask) conditions (see Supplementary Fig. S3). Culture durations in 2D or 3D collagen ranged from 5 to 14 days, depending on the proliferation rate of each cell line (as detailed in Fig. 1). Cells previously cultured on 2D collagen substrates or plastic exhibited a broad, well-spread morphology and a larger cell–matrix contact area, consistent with established 2D-adapted phenotypes. In contrast, cells retrieved from 3D collagen matrices displayed marked morphological changes, including a pronounced reduction in spreading area, particularly evident in HMC3 microglia, while LN229 and T98G glioblastoma cells showed more modest decreases in cell area.

These findings are consistent with previous reports demonstrating that substrate dimensionality and stiffness regulate cell spreading, focal adhesion maturation, and cytoskeletal organization [103–105]. Our study extends these principles to LN229 and T98G glioblastoma cells and HMC3 microglia by providing the first systematic quantification of focal adhesion dynamics and cell mechanics following culture in 2D or 3D collagen environments (Fig. 4 & Table 2). This analysis reveals cell line–specific adaptations and heterogeneity in focal adhesion organization, offering novel insights into how dimensional culture history shapes the mechanical phenotypes of glioblastoma and microglial cells.

Immunostaining for vinculin revealed distinct focal adhesion characteristics between 2D- and 3D-cultured cells across all three cell lines. In 2D, cells exhibited larger, more mature focal adhesions, typically localized at the cell periphery and associated with prominent actin stress fibers. By contrast, cells retrieved from 3D collagen matrices showed smaller, more punctate focal adhesions with reduced actin fiber formation, consistent with adaptation to a softer, heterogeneous microenvironment. The quantification of focal adhesion has been summarized in Table 2 (A-C).

Quantitative analysis revealed marked differences in the average cell spreading area, focal adhesion (FA) number, and FA area between cells cultured in 2D and 3D collagen environments, with the magnitude and significance of these changes varying across cell lines (Fig. 4C–E; Table 2A–C). In HMC3 cells, 3D collagen culture significantly reduced cell area, FA number, and FA area compared to 2D, all with large to huge effect sizes (Table 2). Cell area decreased by ~68 %, FA number dropped by more than half, and FA area was similarly reduced, indicating strong biological effects despite the marginal p-value for FA number. Similarly, in LN229 cells, reductions were also observed across all three metrics, reflecting a robust response to dimensionality. The cell area decreased significantly, FA number and FA area dropped substantially, consistent with a pronounced adaptation to the 3D environment. In contrast, T98G cells showed a significant reduction in cell area after 3D culture, but changes in FA number and FA area were not statistically significant ($p > 0.05$). Nonetheless, both metrics exhibited medium to large effect sizes ($r = 0.250$, $d = 1.502$), suggesting potential trends that may become significant with larger sample sizes. Together, these findings highlight cell line-specific mechanobiological adaptations following culture in 2D and 3D collagen environments, underscoring the value of reporting both statistical significance and effect sizes to fully capture biologically meaningful changes, particularly in studies with limited statistical power.

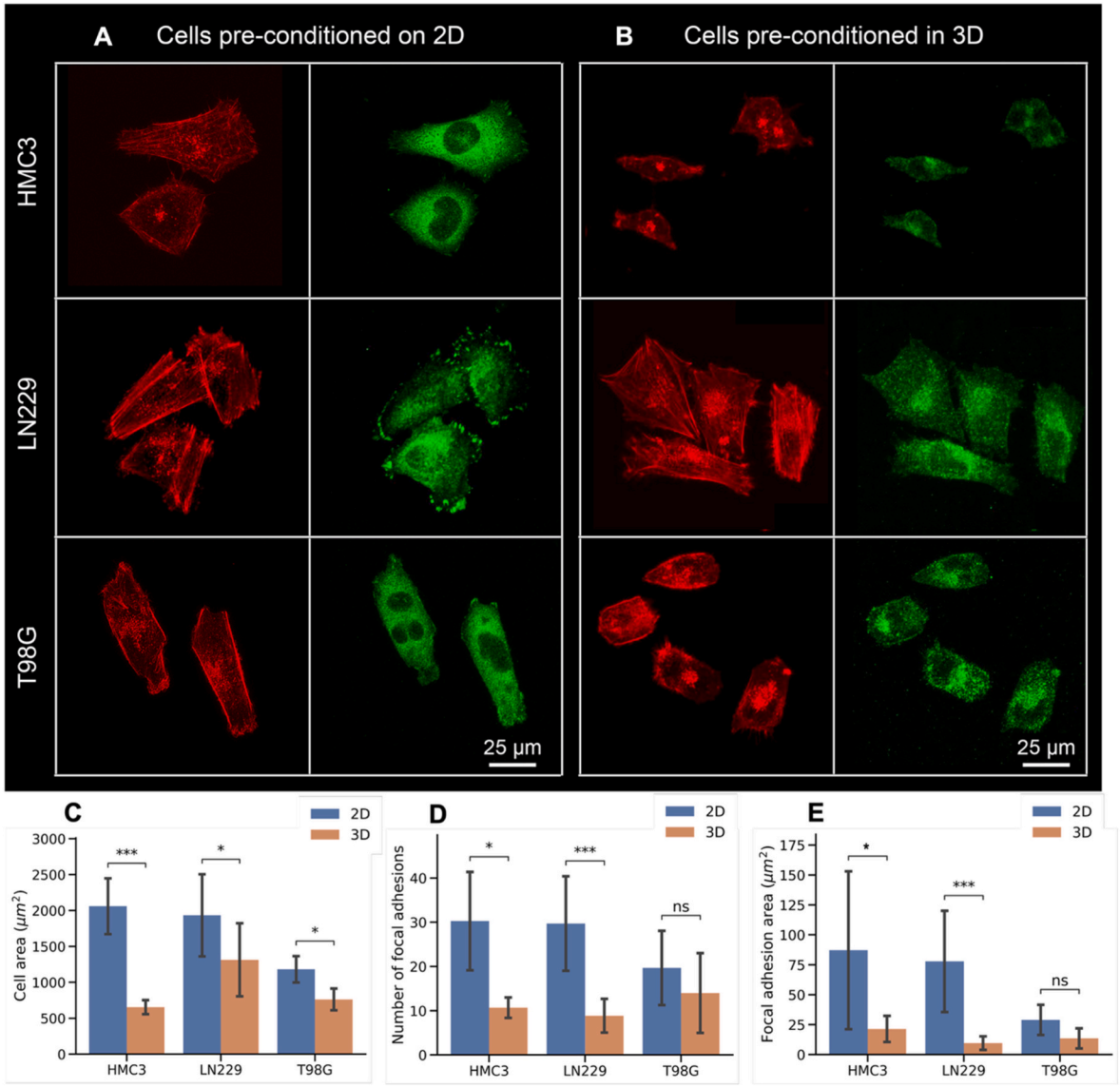

Fig. 4. Changes in the number of focal adhesions based on cytoskeleton images of HMC3, LN229, and T98G cells seeded on glass coverslips after culturing them on 2D collagen-based surfaces (A) and 3D collagen-based bioactive matrices (B). In these images, red staining indicates the presence of F-actin, while green staining displays focal adhesions (i.e., vinculin). Based on these images, cell area (C), the number of focal adhesions per cell (D), and the focal adhesion area (E) were calculated. In the last three images, blue bars correspond to cells pre-conditioned on 2D collagen-coated surfaces, while orange bars represent values obtained from cells cultured in 3D collagen-based bioactive matrices. Statistical analysis was performed using the Welch's *t*-test for normally distributed data and the Mann-Whitney *U* test for non-normally distributed data. Significance levels: *p < 0.05, **p < 0.01, and ***p < 0.001.

The data shown in Fig. 4 & Table 2 indicate that HMC3 microglia cells adjust their adhesion and morphology when transitioning from rigid to soft 3D environments, consistent with their known mechanosensitivity and ability to adopt low-adhesion, amoeboid-like behavior on soft matrices [98,106]. These findings are consistent with microglia's known ability to modulate migration style and adhesion according to ECM topography and mechanical cues [56,100,107].

Whereas, LN229 cells, despite maintaining stress fiber–associated morphology, suggest compensatory mechanisms such as increased integrin turnover [108–110] or unique surface charge properties [111], previously described for this cell line. These findings suggest that LN229 cells maintain their attachment after 3D culture by shifting to a more dynamic adhesion state, minimizing large focal adhesions despite retaining some spread morphology relative to other glioblastoma cell lines.

Conversely, T98G may be less sensitive to dimensionality compared to LN229, which we interpret to be consistent with reports of stable integrin expression (α1β1, α2β1) and decoupling of biochemical and mechanical responses in this cell line [112]. This may indicate that such properties may support the invasive phenotype of T98G by enabling adaptation to mechanical heterogeneity while preserving adequate adhesion dynamics.

Qualitative assessment of vinculin and actin immunostaining (see Fig. 4A and B and Supplementary Information 3) supported our quantitative focal adhesion analysis. Together, these findings illustrate how glioblastoma and microglial cells differentially modulate their adhesion machinery in response to dimensional and mechanical cues, reflecting their distinct roles in the tumor microenvironment. The greater ECM responsiveness of microglia may reflect their immune surveillance role [56,99,100,107]. Whereas the reduced mechanosensitivity of glioblastoma cells might be an indication to support their invasive behavior through durotaxis, blebbing-driven migration, and adaptation to aligned collagen fibrils [113–118]. These mechanistic insights may inform future strategies for targeting tumor invasion and modulating microglial

Table 2
Summary of focal adhesion quantification for HMC3, LN229, and T98G cells cultured in 2D and 3D environments. Data include (A) cell area (μm^2), (B) Average number of focal adhesions (FA), and (C) Average focal adhesion (FA) area (μm^2), reported as mean(M) ± SD or median(Mdn) ± MAD, with corresponding sample size (n), p-values, and effect sizes (Cohen's d or rank biserial correlation r) after performing the Shapiro–Wilk test to assess the normality of the data. (see Supplementary Table S2).

A						
Cell Line	2D (n)	3D (n)	Cell area (μm^2, 2D)	Cell Area (μm^2, 3D)	p-value	Effect Size
			M ± SD			d
HMC3	8	3	2058.74 ± 389.39	653.56 ± 97.81	<0.001	4.055
LN229	10	7	1933.00 ± 570.97	1313.16 ± 508.58	0.034	1.133
T98G	3	4	1180.69 ± 183.34	761.63 ± 151.31	0.034	2.542
B						
Cell Line	2D (n)	3D (n)	FA Number (2D)	FA Number (3D)	p-value	Effect Size
			Mdn ± MAD			r
HMC3	8	3	31.00 ± 5.00	12.00 ± 0.00	0.051	0.833
LN229	10	7	32.00 ± 5.00	8.00 ± 1.00	0.001	0.971
T98G	3	4	24.00 ± 1.00	14.00 ± 6.00	0.721	0.250
C						
Cell Line	2D (n)	3D (n)	FA Area (μm^2, 2D)	FA Area (μm^2, 3D)	p-value	Effect Size
			M ± SD			d
HMC3	8	3	87.10 ± 65.91	21.38 ± 10.98	0.026	1.126
LN229	10	7	77.77 ± 42.24	9.55 ± 5.66	<0.001	2.073
T98G	3	4	28.96 ± 12.60	13.49 ± 8.43	0.154	1.502

function within the glioblastoma niche.

To further characterize how prior dimensional environments influence cellular mechanics beyond adhesion dynamics, we next examined the intrinsic mechanical properties of the cells themselves. Specifically, we measured the stiffness (Young's modulus) of HMC3, LN229, and T98G cells using single-cell nanoindentation after culture under three different conditions: conventional plastic flasks (control), collagen type-I–coated 2D surfaces, or collagen type-I 3D scaffolds (Fig. 5). We found no significant difference in stiffness for HMC3 and LN229 cells between 2D and 3D pre-culture conditions. In contrast, T98G cells exhibited a significant reduction in Young's modulus after 3D collagen culture compared to 2D.

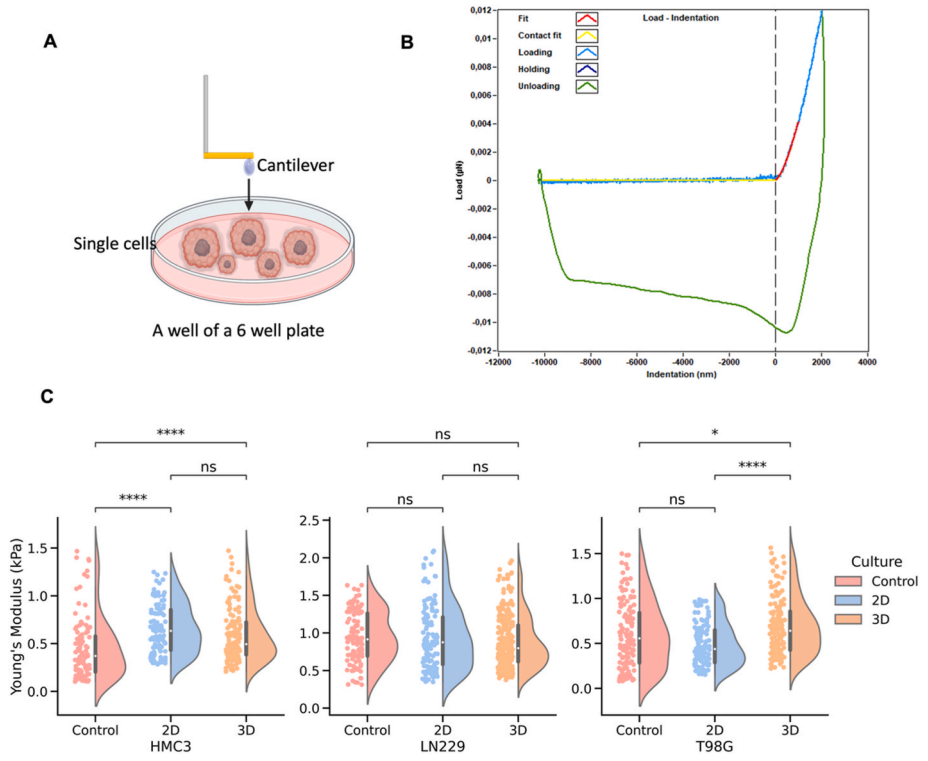

Fig. 5. A) A schematic of the nanoindentation experiment is presented [119] detailing indentation on single cells conducted using a cantilever with a spherical tip. B) Representative load–indentation curves featuring Hertz fits. C) Stiffness measurements obtained through the peak load poking mode of the nanoindenter on cells. The elasticity (Young's modulus) of HMC3, LN229, and T98G was analyzed using the single-cell nanoindentation method. Similar to other mechanical characterizations, these cell lines underwent specific culture pre-culture conditions, i.e., a 2D hard substrate and a 3D soft substrate, along with a conventional culture flask serving as the control. Mann-Whitney *U* Test was conducted for statistical analysis among the three conditions, where *p < 0.05, **p < 0.01, ***p < 0.001, and ****p < 0.0001.

Considering the difference in Young's Modulus of both glioblastoma cell lines, LN229 shows no statistically significant difference between 2D and 3D precultured conditions, as compared to T98G (Fig. 5C & Table 3).

LN229 cells have been reported to show minimal changes in morphology and mechanics between 2D and 3D culture conditions [120]. As shown in Fig. 2, LN229 also showed similar behavior across all three culture conditions in terms of proliferation. This suggests that these cells possess a more adaptable cytoskeletal architecture, which may explain the lack of significant stiffness differences among control, 2D, and 3D pre-culture conditions. These findings align with the TFM results, where LN229 exhibited only modest differences between 2D and 3D pre-culture conditions compared to the more pronounced changes seen in T98G.

By contrast, T98G cells displayed a prominent difference in cellular stiffness between 2D and 3D pre-culture conditions (Fig. 5C & Table 3). Studies on glioblastoma models and reviews on 3D culture systems have emphasized that a more *in vivo*-like microenvironment in 3D culture can drive cytoskeletal tension and focal adhesion reinforcement [4,57,121,122], which may explain why T98G cells become stiffer in 3D pre-culture conditions. Supplementary Fig. 3 further supports this, showing that T98G cells appear to have greater cytoskeletal remodeling, which is often associated with higher cellular stiffness [123–125].

Our findings suggest that HMC3 cells do not show significant differences in stiffness between 2D and 3D pre-culture conditions (Fig. 5C & Table 3), similar to TFM results, which aligns with the notion that microglia maintain a stable mechanical phenotype across different dimensionalities. Notably, qualitative immunostaining images (see Supplementary Fig. S3) demonstrate the greater cytoskeletal remodeling of HMC3 between 2D and 3D pre-culture conditions, indicating that microglia are probably more sensitive to environmental cues at the structural level without a corresponding change in mechanical stiffness. This apparent discrepancy may reflect the unique ability of microglia to adapt their morphology dynamically while maintaining consistent mechanical properties, as suggested by previous studies [97,107,126,127]. To gain a comprehensive understanding of microglial mechanical properties in varying culture conditions, further research involving direct stiffness measurements is necessary.

Despite probing the same cells, our three assays reveal distinct but interrelated aspects of cellular mechanobiology. Traction force microscopy (TFM) measures the contractile forces transmitted to the extracellular matrix (ECM) through cell–matrix adhesions [40,128]. Focal adhesion (FA) quantification reflects the size, number, and area of integrin-based complexes that mediate cell–ECM attachment [129]. Stiffness (Young's modulus, YM) measured by nanoindentation primarily reflects the mechanical resistance of the cell body (cortical actin and nucleus) [130].

As a general principle, these three readouts tend to correlate positively. Larger focal adhesions are often associated with stronger traction forces [131], and cells typically exhibit higher stiffness when cultured on stiffer substrates [132,133]. Tissue cells also tend to migrate towards stiffer substrates, presumably because adhesions develop more effectively on the stiffer side [134]. However, since these processes involve overlapping, but still distinct structural and signaling pathways, they are not strictly coupled. In particular, small adhesions can also exert large traction forces, especially during periods of migration and growth, underscoring that adhesion size alone does not dictate force output [135,136]. Indeed, Oakes et al. demonstrated that traction force magnitude does not directly correlate with FA size or composition, showing that small adhesions can sustain large traction stresses [137,138]. Similarly, studies by Rheinlaender et al. show cell stiffness can increase through cortical actin crosslinking independent of traction force output [139]. Moreover, direct interference with mechanotransductive signaling, such as siRNA-mediated kinase knockdown, can decouple traction forces, adhesion dynamics, and cellular stiffness [140].

Thus, our data showing that each assay responds differently in each cell line are not inconsistent, but rather highlight the complex, multidimensional nature of mechanobiological adaptation. HMC3 microglia remodel adhesion size and spread area in 3D but maintain stable traction and stiffness, reflecting similar behavior to podosomes [141] and mirroring observations in other myeloid-lineage cells, osteoclasts [142], and monocytes [143], where podosome clusters generate primarily vertical, protrusive forces with minimal net lateral traction despite extensive adhesion assembly. T98G glioblastoma cells amplify both traction and stiffness after 3D embedding, despite minimal focal adhesion growth, which refers to studies showing FAs can transmit six-fold higher tension without requiring further growth, demonstrating the non-linear relationship between these parameters [136]. In contrast, LN229 glioblastoma cells adjust adhesion architecture and traction, but preserve cortical stiffness, reflecting a cortex-vs-stress-fiber decoupling [139]. Such intratumoral mechanobiological heterogeneity mirrors broader findings that cancer cells often uncouple stiffness from traction force generation [144].

3D collagen environments generate smaller, more dynamic adhesions than 2D surfaces [145], yet cells can sustain force via alternative transmission modes, underlining why FA number/area and traction don't always align. Finally, statistical significance alone can overlook biologically meaningful changes when n is low. For our focal-adhesion data (the smallest sample size), we therefore report effect sizes (Cohen's d) alongside p-values (Table 1, Fig. 3). For example, HMC3 FA number ($p = 0.051$) has $d = 0.83$, indicating a large difference despite borderline significance [146].

Table 3
Mean Young's modulus (kPa) of single cells cultured under three different conditions: conventional tissue culture plastic (control), collagen type I–I-coated 2D surfaces, and collagen type I–I-based 3D scaffolds. Data are presented as n = X cells per condition from Y independent experiments. Statistical comparisons were performed using the nonparametric Mann–Whitney *U* test.

Cell	Culture	X	Y	Young's modulus (kPa)
HMC3	Control	116	4	0.45 ± 0.03
HMC3	2D	125	4	0.65 ± 0.02
HMC3	3D	149	6	0.59 ± 0.02
LN229	Control	127	4	0.94 ± 0.03
LN229	2D	145	6	0.94 ± 0.04
LN229	3D	290	6	0.88 ± 0.02
T98G	Control	150	4	0.59 ± 0.03
T98G	2D	140	4	0.49 ± 0.02
T98G	3D	165	6	0.69 ± 0.03

3. Conclusions

In summary, our study demonstrates that the dimensionality of the pre-culture environment imparts a mechanical memory to glioblastoma cells that persists even when they are reseeded onto standardized 2D surfaces. This supports our hypothesis that cells retain biomechanical imprints of their previous 2D or 3D microenvironments. Specifically, T98G glioblastoma cells exhibit a pronounced memory effect, displaying significantly lower traction forces and strain energy after 3D pre-culture, alongside marked differences in cellular stiffness, despite statistically unchanged focal adhesion number and area. Whereas, LN229 glioblastoma cells, adjust their adhesion architecture and traction output in response to dimensionality shifts while preserving cortical stiffness, reflecting a distinct, cell–type–specific adaptation strategy. In comparison, HMC3 microglia show minimal evidence of mechanical memory, maintaining stable traction forces and stiffness across pre-culture conditions despite modest but significant changes in focal adhesion number and size, and pronounced changes in cell spread area. These findings highlight the heterogeneity of mechanoadaptation between malignant and non-malignant brain-resident cells.

These findings emphasize that traction force generation, focal-

adhesion quantification, and cortical stiffness each report on separate facets of the cell's force-generation machinery and do not necessarily always correlate in the same manner. This decoupling is consistent with prior reports showing that mature focal adhesions can bear high tension without further growth, and that nanoindentation primarily probes the apical cortex rather than deeper stress fibers. By quantifying all three parameters and consistently reporting p-values, we captured biologically meaningful, cell line-specific responses. For the focal adhesion assay, where sample sizes were more limited, we complemented this with effect size analysis to strengthen the interpretation.

Ultimately, our work highlights the importance of accounting for mechanical memory and cell type heterogeneity in *in vitro* models of glioblastoma mechanobiology. Incorporating 3D bioactive matrices into experimental workflows and examining how pre-culture conditions influence subsequent 2D assays offers additional insight into tumor-microenvironment interactions. While astrocytes or neural stem cells are often used as lineage controls for glioblastoma, our inclusion of HMC3 microglia specifically probes the distinct mechanics of non-malignant niche cells rather than tumorigenic lineage differences. We anticipate that this multi-assay, pre-culture, and reseeding approach can inform future studies on glioblastoma progression and interactions with the microenvironment.

4. Materials and methods

4.1. Cell culture

Human-derived malignant GB cells LN229 (ATCC-CRL-2611, Germany), T98G (ATCC-CRL-1690, Germany), and human microglia cells HMC3 (ATCC CRL-3304, Germany) were maintained and cultured in Dulbecco's Modified Eagle Medium (DMEM), supplemented with 10 % v/v fetal bovine serum (FBS, PAN-Biotech Gmb, Aidenbach, Germany), 1 % penicillin-streptomycin (Sigma Life science, St. Louis, USA), 1.0 % v/v Glutamax (Gibco, New York, US) and 0.1 % v/v Gentamicin (Gibco, New York, US) in T75 culture flasks (SARSTEDT AG & Co.KG, Nümbrecht, Germany). All cultures were maintained at 37 °C with 5.0 % v/v CO_2 in an incubator (Heracell vios 160i; Thermo scientific, Waltam, US). The cells were regularly split with accutase (PAN-Biotech Gmb, Aidenbach, Germany) in growing periods of 3–5 days, previously washed with Dulbecco's Phosphate Buffered Saline Modified (DBPS; Sigma Life science, St. Louis, USA) twice.

4.2. 2D collagen matrix

To coat 6-well plates with collagen, 0.1 M NaOH, 10X PBS, 1X DPBS, and 3.5 mg/mL collagen type I from rat tail (ibidi GmbH; Gräfelfing, Germany) were mixed [147]. Further, to obtain a neutral pH, 3.17 mL of the mixed solution was added per well in a 6-well plate and spread gently to have a uniform collagen coating. This well plate was then left in the incubator to polymerize overnight at 37 °C. After polymerization, the 6 well plates were transferred to the sterile hood and dried for 48 hours. In the end, the collagen coating was washed three times with sterile Milli Q water for 30 mins intervals. After removing sterile water from the 2D collagen coatings, 10,000 cells/well were seeded and left for incubation under cell culture conditions.

4.3. 3D collagen matrix

3.5 mg/mL collagen type I, DMEM, the reconstruction buffer, and 1M NaOH were mixed to prepare a 3D collagen scaffold at neutral pH [148]. The reconstruction buffer was prepared by mixing (0.044 g of sodium bicarbonate (Sigma-Germany) in 0.4 mL of HEPES (Sigma, Germany)) and 1.6 mL of Milli Q water and then filtered the solution with a 0.2 μm filter (FP 30/0.2 CA-S, sterile, Whatman TM, US). While this mixture was placed on ice to slow down the polymerization process, the cells were split, counted, and resuspended to get a final cell concentration of 10,000 cells/well of a 96-well plate for all three cell lines (HMC3, LN229, and T98G). Cells resuspended in DMEM were added to the collagen gel mixture and mixed well, avoiding bubbles. In the end, 0.2 mL of collagen-cell mixture was added per well. After 30 min of incubation to facilitate collagen polymerization, DMEM was added to these 3D collagen scaffolds and then placed in the incubator to facilitate cell growth. Cell culture media was changed every 48 h.

4.4. Cell proliferation assay

Studies of the cell proliferation were carried out with HMC3, LN229, and T98G cells in three conditions: conventional cell culture as a control, 2D collagen coating, and 3D collagen matrices. For the cell proliferation analysis, 5000 cells/well were seeded on the 24-well plate as a control for 2D conditions and 10,000 cells/well for 3D conditions. Cells were treated with WST-8 (10 % v/v, Thermofisher, Germany) for a 3h incubation period at cell culture conditions to determine the viable cell number and study the induction or inhibition of cell proliferation *in vitro*. Cell proliferation was measured every 24 h, in a plate reader (EPOCH/2 microplate reader; BioTek, Winooski, US) at room temperature, and the absorbance was read at 450 nm. After such a measurement, cells were washed twice with DPBS, DMEM was added, and cells were left under cell culture conditions again. This strategy was repeated for 14 days with the same samples. Proliferation assays were carried out in triplicate.

4.5. Preparation of polyacrylamide gels for single-cell traction force microscopy

Since the mechanical properties of polyacrylamide (PAA) gels are easily tunable, these gels are widely used for single-cell traction force microscopy (TFM) [36]. For TFM measurements, flat PAA gels coated with ECM protein, i.e., collagen type I (ibidi GmbH, Germany), were prepared following protocols previously described in the literature [79, 149]. These gels were prepared with a target Young's modulus of 3.13 ± 0.42 kPa [64] and characterized using a commercially available fiber-optics-based nanoindenter (Pavone, Optics11, Netherlands) [150, 151] with a spherical probe (radius = 8.5 μm, spring constant = 0.32 N/m). A 7 × 7 matrix scan protocol was employed to assess gel uniformity and validate linear elasticity assumptions required for traction force microscopy. (see Supplementary Information 1 for detailed characterization). FluoSpheres™ Carboxylate-Modified Microspheres (red, 200 nm in diameter, F8787, Thermofisher, Germany) were used as a fiducial marker embedded in the 50–70 μm thick layer of PAA gel. These collagen-coated PAA gels were washed with sterile DPBS before seeding the cells. All cell lines cultured in 2D and 3D environments were extracted using collagenase (1.44 mg/mL in PBS). Approximately 20, 000 cells per gel were seeded and incubated overnight at 37 °C in a humidified incubator with 5.0 % CO_2 to ensure adhesion. Non-adherent cells were gently removed by washing the gels with pre-warmed DPBS, and 3 mL DMEM was added to each gel. Cells were stained with 1.0 μL (per sample) of Calcein, AM (2261443, 1 mM), and nuclei with 1.0 μL/mL Hoechst (33342, 20 mM) for live-cell imaging.

4.6. TFM imaging and analysis

Confocal images of cells were taken in two states. 1. Stressed state, i.e., when cells were adhered to the collagen-coated PAA gels, referred to as the cell image. 2. Relaxed state, i.e., when cells were not adherent anymore after adding accutase to the collagen-coated PAA gels, referred to as the reference image. Imaging was performed using a Nikon A1R confocal microscope with a Nikon Plan Fluor 40× objective (NA 1.3, OI (WD 0.2 mm, FOV 0.32 × 0.32 mm)) to perform TFM. The voxel size was 0.27 μm × 0.27 μm × 0.9 μm (512 × 512 pixels, z-resolution: 0.9 μm). The integer drift between the cell and reference image was determined using cross-correlation. The images were then cropped to only contain

the overlapping section between the images. From the Z-stacks, the plane containing the most beads was chosen based on the sharpness of the image. This plane was combined with the two planes above and below to yield a 2D image containing the beads on the surface of the gel. Bead displacements were calculated using the pyramidal Kanade-Lucas-Tomasi (KLT) tracking algorithm [152,153], a direct optical flow method for determining displacement fields between image pairs [35,45,154]. The KLT algorithm was chosen over PIV and PTV due to higher accuracy and robustness for tracking small, local bead displacements in densely labeled TFM samples [155,156]. This ensures the reliability and resolution of the traction force data presented in this work. Traction forces were reconstructed using regularized Fourier Transform Traction Cytometry (FTTC), an inverse method that estimates cellular traction forces from measured substrate displacements. A regularization scheme was applied to address the ill-posed nature of the inverse problem, which characterizes the traction stress field from displacement data using L2 (Tikhonov) regularization to mitigate noise-related artifacts. The regularization parameter (λ) was optimized for each dataset to balance noise suppression with spatial resolution [34–36,45,157,158]. The traction stress of each cell was characterized by the total strain energy stored in the PAA gel due to cell tractions, which is calculated as the product of local tractions and deformations integrated over the spreading area of the cells. Average traction stress was normalized to respective cell areas to determine the average force/area of a single cell. The forces exerted at individual focal adhesions were analyzed in terms of mean focal adhesion stress (determined by selecting visible focal adhesions from the traction stress map). For TFM analysis, three cell types (HMC3, LN229, and T98G) were cultured under 2D and 3D collagen conditions, then reseeded onto polyacrylamide substrates for force measurements. Each condition was independently repeated 5–10 times per cell type, and the total number of single cells analyzed per condition ranged from 85 to 193, as detailed in Table 1 (Results and Discussion section).

4.7. Validation and error analysis

The accuracy of our traction force reconstruction methodology, implemented using the code provided by J. Blumberg & U.Schwarz [34], has been systematically benchmarked against synthetic ground-truth data in previous work. In particular, Blumberg et al. performed extensive simulations with analytically defined traction patterns under controlled noise conditions, demonstrating that the root mean square (RMS) error in reconstructed tractions is typically <15 % of the peak traction for well-resolved features under realistic noise and sampling conditions. A detailed summary of these published validation results, including the effects of noise and regularization, is provided in Appendix 1 in the Supplementary Materials.

4.8. Immunofluorescence assay

Immunofluorescence assay (IFA) was performed to investigate the cytoskeleton arrangement of HMC3, LN229, and T98G after 2D and 3D pre-culture conditions, along with conventionally cultured cells as a control. To image vinculin, actin filaments (F-actin), and nuclei, approximately 15,000 cells were cultured on sterilized coverslips overnight and then fixed with 4 % paraformaldehyde (Sigma-Germany) for 20 min at 37 °C and permeabilized with 0.1 % v/v Triton-X-100 (Sigma-Germany) for 10 min. Then, blocking was done with 1.0 % w/v bovine serum albumin (BSA) in 1X phosphate-buffered saline (PBS), and cells were incubated at room temperature for 30 min. Cells were stained for vinculin with primary antibody monoclonal anti-vinculin (V9131, Sigma-Germany) diluted in BSA (1:200). A goat anti-mouse secondary antibody Alexa Fluor™ 488 (SA5-10264, Invitrogen, Germany) diluted in PBS (1:1000) along with a compatible counterstain for the cytoskeleton Rhodamine-Phalloidin (R415, Invitrogen, Germany) and 4′,6-diamidino-2-phenylindole (DAPI) (D1306, Invitrogen, Germany) for the nucleus was used to perform an immunofluorescence assay. A Nikon A1R confocal microscope was used to image the cytoskeletal organization of cells.

4.9. Quantification and characterization of focal adhesions

For focal adhesion analysis, images obtained from the Immunofluorescence assay were processed following the protocol introduced by Horzum et al. [159] With some parameter modifications. However, the same parameters were applied to all images to avoid bias. Image processing was performed in Fiji [160,161].

4.10. Single-cell mechanical characterization

Mechanical properties of single cells after 2D and 3D pre-culture conditioning were measured using a nanoindenter (Pavone, Optics11, Netherlands) [150,151]. Cells were isolated from 2D collagen coatings and 3D collagen matrices and seeded into 6-well glass-bottom plates. Cells were left to adhere overnight (12–16 h) in standard culture conditions (37 °C, 5.0 % CO_2). A spherical nanoindentation probe (tip radius 3.5 μm and spring constant of 0.013 N/m) was calibrated in culture medium (DMEM), and measurements were performed **at 37 °C** to maintain physiological conditions and avoid thermal drift. The probe size was chosen to provide sufficient spatial resolution while minimizing excessive deformation of the cell membrane. Indentation was performed at the nuclear region of the individual cells, with a maximum peak load of 0.012 μN and indentation speed of 1.0 μm/s, using the Peak Load Poking (PLP) mode. The PLP mode operates in an open-loop system where the piezoelectric speed is controlled to achieve a preset maximum load, after which the probe retracts at high speed by the system's default settings [162]. The chosen load and speed parameters minimized cell deformation artifacts while allowing accurate stiffness measurements. Data analysis was conducted with the Data Viewer (V2.5.0) software provided by the manufacturer. Young's modulus was calculated by fitting the load-indentation curves to the Hertzian contact model. The contact point was determined via software-integrated fitting up to 20 % of the maximum load (P_{max}%), and only fits with a coefficient of determination (R^2) ≥ 0.95 were accepted. Calibration of the system was performed regularly to ensure consistent force measurements across samples. The information regarding sample size and independent experiments is detailed in Table 3 (Results and Discussion section).

4.11. Statistical analysis

Experiments for TFM analysis were conducted on different days based on the proliferation rate for each pre-culture condition and cell type. During post-processing, outliers were removed by selecting data within the 5th to 95th percentile. To ensure balanced datasets for statistical analysis, we then randomly sampled the data to match the smallest group size. Statistical significance was assessed using the nonparametric Mann–Whitney *U* test due to non-normal distribution. It was implemented with Python libraries, including SciPy [163], NumPy [164], and Pandas [165,166]. Data visualization was performed using Seaborn [167], with statistical significance annotated via statannotations [168]. The same procedure was applied to the single-cell nanoindentation data, except that random sampling was omitted.

For focal adhesion, after image processing, the results were further analyzed for statistical significance and visualization using Python. Specifically, SciPy was used for statistical significance testing, Pandas for data handling, Seaborn for visualization, and statannotations for statistical annotations. Unlike TFM analysis, focal adhesion data were not randomly sampled due to limited samples, particularly for HMC3 and T98G cell lines. Sample sizes for focal adhesion analysis varied due to experimental constraints. Data normality was assessed using the Shapiro–Wilk test. Depending on the distribution, either the Welch *t*-test with Cohen's *d* as the effect size metric (for normally distributed data) or

a Mann–Whitney *U* test with rank biserial correlation (*r*) as the effect size metric (for non-normally distributed data) was performed to evaluate statistical significance and effect size. *P*-values greater than 0.05 were considered not significant; significance levels were indicated as follows: *for $0.05 > p > 0.01$, ** for $0.01 > p > 0.001$, *** for $0.001 > p > 0.0001$, and **** for $p < 0.0001$.

CRediT authorship contribution statement

Mishal Khan: Writing – original draft, Visualization, Validation, Methodology, Investigation, Formal analysis, Data curation. **Philipp Kollenz:** Software, Investigation, Formal analysis. **Maret Fritzenschaft:** Methodology, Investigation, Formal analysis. **Fereydoon Taheri:** Validation, Supervision, Software, Methodology, Formal analysis. **Federico Colombo:** Supervision, Methodology, Investigation, Formal analysis. **Johannes W. Blumberg:** Validation, Supervision, Software, Methodology, Investigation, Formal analysis. **Luise Schlotterose:** Supervision, Resources. **Ulrich Sebastian Schwarz:** Writing – review & editing, Visualization, Validation, Supervision, Software, Resources, Methodology, Funding acquisition, Formal analysis, Conceptualization. **Aldo Leal-Egaña:** Writing – review & editing, Visualization, Supervision, Methodology, Funding acquisition, Formal analysis, Conceptualization. **Christine Selhuber-Unkel:** Writing – review & editing, Visualization, Supervision, Resources, Project administration, Funding acquisition, Conceptualization.

Declaration of generative AI and AI-assisted technologies in the writing process

During the preparation of this work, the author used Claude, Perplexity, and ChatGPT to refine the writing process. However, the intellectual contributions and conceptual developments are entirely those of the authors. After using Claude, Perplexity, and ChatGPT, the author reviewed and edited the content as needed and takes full responsibility for the content of the published article.

Funding sources

I declare that this work was funded by the German Research Foundation (DFG) as part of the Research Training Group "Materials4Brain" (RTG2154). We also acknowledge funding by the DFG under Germany's Excellence Strategy - EXC 2082/1–390761711 (the Karlsruhe-Heidelberg cluster of excellence 3DMM2O) to U.S.S. and C.S., as well as through DFG grant LE3418/4-1 to A.L-E, and the Carl Zeiss Foundation to J.B. U. S. S. and C. S. are supported by the Max Planck School Matter to Life supported by the German Federal Ministry of Education and Research (BMBF). We also acknowledge support through the DFG SPP 2332, the Volkswagen Foundation (Life?, Az. 96733), and the European Research Council (CoG PHOTOMECH, Grant no. 101001797).

Declaration of competing interest

The authors declare that they have no known competing financial interests or personal relationships that could have appeared to influence the work reported in this paper.

Acknowledgments

We would like to thank the soft (bio)materials characterization Core Facility (Biomechanics) funded by the Federal Ministry of Education and Research (BMBF) and the Ministry of Science Baden-Württemberg within the framework of the Excellence Strategy of the Federal and State Governments of Germany. The authors thank the Nikon Imaging Center in Heidelberg for their imaging facility and support. The HMC3 cell line was generously provided by Dr. Kirsten Hattermann (Institute of Anatomy, University of Kiel). LN229 and T98G were generously provided by Prof. Dr. Janka Held-Feindt (Department of Neurosurgery, University Medical Center Schleswig-Holstein UKSH, Campus Kiel) and Dana Hellmold supported in LN229 and T98G handling. Figs. 1, 3A and 5A and the graphical abstract were created using BioRender.com.

Appendix A. Supplementary data

Supplementary data to this article can be found online at https://doi.org/10.1016/j.bioactmat.2025.09.025.

References

[1] D. Friedmann-Morvinski, Glioblastoma Heterogeneity and Cancer Cell Plasticity, 2014, https://doi.org/10.1615/critrevoncog.2014011777.
[2] T.T. Lah, M. Novak, B. Breznik, Brain Malignancies: Glioblastoma and Brain Metastases, Academic Press, Feb. 01, 2020, https://doi.org/10.1016/j.semcancer.2019.10.010.
[3] J.V. Joseph, M.S. Blaavand, T. Daubon, F.A. Kruyt, M.K. Thomsen, Three-Dimensional Culture Models to Study Glioblastoma — Current Trends and Future Perspectives, Elsevier Ltd., Dec. 01, 2021, https://doi.org/10.1016/j.coph.2021.08.019.
[4] P. Sharma, A. Aaroe, J. Liang, V.K. Puduvalli, Tumor microenvironment in glioblastoma: current and emerging concepts, Neurooncol. Adv. 5 (1) (Jan. 2023), https://doi.org/10.1093/noajnl/vdad009.
[5] X. Zhang, K. Ding, J. Wang, X. Li, P. Zhao, Chemoresistance Caused by the Microenvironment of Glioblastoma and the Corresponding Solutions, Elsevier Masson SAS, Jan. 01, 2019, https://doi.org/10.1016/j.biopha.2018.10.063.
[6] V. Di Nunno, E. Franceschi, A. Tosoni, L. Gatto, S. Bartolini, A.A. Brandes, Glioblastoma Microenvironment: from an Inviolable Defense to a Therapeutic Chance, Frontiers Media S.A, Mar. 02, 2022, https://doi.org/10.3389/fonc.2022.852950.
[7] N.A. Charles, E.C. Holland, R. Gilbertson, R. Glass, H. Kettenmann, The brain tumor microenvironment, Glia 59 (8) (Aug. 2011) 1169–1180, https://doi.org/10.1002/glia.21136.
[8] Y.A. Miroshnikova, et al., Tissue mechanics promote IDH1-dependent HIF1α-tenascin C feedback to regulate glioblastoma aggression, Nat. Cell Biol. 18 (12) (Dec. 2016) 1336–1345, https://doi.org/10.1038/ncb3429.
[9] A.A. Ketebo, C. Park, J. Kim, M. Jun, S. Park, Probing mechanobiological role of filamin A in migration and invasion of human U87 glioblastoma cells using submicron soft pillars, Nano Converg 8 (1) (2021) 19.
[10] B.M. Rubenstein, L.J. Kaufman, The role of extracellular matrix in glioma invasion: a cellular potts model approach, Biophys. J. 95 (12) (Dec. 2008) 5661–5680, https://doi.org/10.1529/biophysj.108.140624.
[11] K. Pogoda, et al., Soft substrates containing hyaluronan mimic the effects of increased stiffness on morphology, motility, and proliferation of glioma cells, Biomacromolecules 18 (10) (Oct. 2017) 3040–3051, https://doi.org/10.1021/acs.biomac.7b00324.
[12] J.S. So, H. Kim, K.S. Han, Mechanisms of Invasion in Glioblastoma: Extracellular Matrix, Ca2+ Signaling, and Glutamate, Frontiers Media S.A., Jun. 02, 2021, https://doi.org/10.3389/fncel.2021.663092.
[13] M. Wiranowska and M. V Rojiani, 'Extracellular Matrix Microenvironment in Glioma Progression'. doi: 10.5772/24666.
[14] D. Sood, et al., 3D extracellular matrix microenvironment in bioengineered tissue models of primary pediatric and adult brain tumors, Nat. Commun. 10 (1) (Dec. 2019), https://doi.org/10.1038/s41467-019-12420-1.
[15] E. Mohiuddin, H. Wakimoto, Extracellular Matrix in Glioblastoma: Opportunities for Emerging Therapeutic Approaches, 2021.
[16] A.G. Bhargav, J.S. Domino, R. Chamoun, S.M. Thomas, Mechanical Properties in the Glioma Microenvironment: Emerging Insights and Theranostic Opportunities, Frontiers Media S.A, Jan. 21, 2022, https://doi.org/10.3389/fonc.2021.805628.
[17] V.A. Cuddapah, S. Robel, S. Watkins, H. Sontheimer, A Neurocentric Perspective on Glioma Invasion, Nature Publishing Group, 2014, https://doi.org/10.1038/nrn3765.
[18] A. Vollmann-Zwerenz, V. Leidgens, G. Feliciello, C.A. Klein, P. Hau, Tumor Cell Invasion in Glioblastoma, MDPI AG, Mar. 02, 2020, https://doi.org/10.3390/ijms21061932.
[19] P. Beauchesne, Extra-Neural Metastases of Malignant Gliomas: Myth or Reality?, Mar. 2011, https://doi.org/10.3390/cancers3010461.
[20] A.F. Haddad, et al., Mouse models of glioblastoma for the evaluation of novel therapeutic strategies, Neurooncol. Adv. 3 (1) (Jan. 2021) vdab100, https://doi.org/10.1093/noajnl/vdab100.
[21] L. Neufeld, et al., Microengineered perfusable 3D-bioprinted glioblastoma model for in vivo mimicry of tumor microenvironment [Online]. Available: https://www.science.org, 2021.
[22] M. Kapałczyńska, et al., 2D and 3D cell cultures – a comparison of different types of cancer cell cultures, Arch. Med. Sci. 14 (4) (2018) 910–919, https://doi.org/10.5114/aoms.2016.63743.
[23] C.K. Mo, et al., Tumour evolution and microenvironment interactions in 2D and 3D space, Nature 634 (8036) (Oct. 2024) 1178–1186, https://doi.org/10.1038/s41586-024-08087-4.
[24] M. M. Biotechnologie, 'Proliferation Behaviour of Glioblastoma in 2D and 3D Collagen Systems'.

[25] T. Stanković, et al., In vitro biomimetic models for glioblastoma-a promising tool for drug response studies, Drug Resist. Updates 55 (Mar) (2021), https://doi.org/10.1016/j.drup.2021.100753.
[26] W. Xiao, A. Sohrabi, S.K. Seidlits, Integrating the glioblastoma microenvironment into engineered experimental models, Future Medicine Ltd (2017), https://doi.org/10.4155/fsoa-2016-0094.
[27] K. M. Yamada and E. Cukierman, 'Modeling Tissue Morphogenesis and Cancer in 3D', Aug. 24, 2007, Elsevier B.V. doi: 10.1016/j.cell.2007.08.006.
[28] L.J. Kaufman, et al., Glioma expansion in collagen I matrices: analyzing collagen concentration-dependent growth and motility patterns, Biophys. J. 89 (1) (2005) 635–650, https://doi.org/10.1529/biophysj.105.061994.
[29] I.R. Calori, S.R. Alves, H. Bi, A.C. Tedesco, Type-I collagen/collagenase modulates the 3D structure and behavior of glioblastoma spheroid models, ACS Appl. Bio Mater. 5 (2) (Feb. 2022) 723–733, https://doi.org/10.1021/acsabm.1c01138.
[30] Y.L. Yang, S. Motte, L.J. Kaufman, Pore size variable type I collagen gels and their interaction with glioma cells, Biomaterials 31 (21) (Jul. 2010) 5678–5688, https://doi.org/10.1016/j.biomaterials.2010.03.039.
[31] L. Yao, K. Tran, D. Nguyen, Collagen matrices mediate glioma cell migration induced by an electrical signal, Gels 8 (9) (Sep. 2022), https://doi.org/10.3390/gels8090545.
[32] D. Böhringer, et al., Fiber alignment in 3D collagen networks as a biophysical marker for cell contractility, Matrix Biol. 124 (Dec. 2023) 39–48, https://doi.org/10.1016/j.matbio.2023.11.004.
[33] A.S. Vanina, A.V. Sychev, E.V. Grekhnyova, E.B. Postnikov, A collagen network-based hydrogel phantom for testing models of the metabolite transport in the brain parenchyma, in: Proceedings - 4th International Conference 'Neurotechnologies and Neurointerfaces', CNN 2022, Institute of Electrical and Electronics Engineers Inc., 2022, pp. 212–214, https://doi.org/10.1109/CNN56452.2022.9912549.
[34] J.W. Blumberg, U.S. Schwarz, Comparison of direct and inverse methods for 2.5D traction force microscopy, PLoS One 17 (1 January) (Jan. 2022), https://doi.org/10.1371/journal.pone.0262773.
[35] J. Christian, et al., Control of cell adhesion using hydrogel patterning techniques for applications in traction force microscopy, JoVE J. 2022 (179) (Jan. 2022), https://doi.org/10.3791/63121.
[36] U.S. Schwarz, J.R.D. Soiné, Traction Force Microscopy on Soft Elastic Substrates: a Guide to Recent Computational Advances, Elsevier, Nov. 01, 2015, https://doi.org/10.1016/j.bbamcr.2015.05.028.
[37] M. Lekka, K. Gnanachandran, A. Kubiak, T. Zieliński, J. Zemła, Traction Force Microscopy – Measuring the Forces Exerted by Cells, Elsevier Ltd., Nov. 01, 2021, https://doi.org/10.1016/j.micron.2021.103138.
[38] P. Roca-Cusachs, V. Conte, X. Trepat, Quantifying Forces in Cell Biology, Nature Publishing Group, Jul. 01, 2017, https://doi.org/10.1038/ncb3564.
[39] S.V. Plotnikov, B. Sabass, U.S. Schwarz, C.M. Waterman, High-resolution traction force microscopy, in: Methods in Cell Biology, 123, Academic Press Inc., 2014, pp. 367–394, https://doi.org/10.1016/B978-0-12-420138-5.00020-3.
[40] A.K. Denisin, H. Kim, I.H. Riedel-Kruse, B.L. Pruitt, Field Guide to Traction Force Microscopy, Springer, Apr. 01, 2024, https://doi.org/10.1007/s12195-024-00801-6.
[41] A. Zancla, P. Mozetic, M. Orsini, G. Forte, A. Rainer, A primer to traction force microscopy. American Society for Biochemistry and Molecular Biology Inc, May 01, 2022, https://doi.org/10.1016/j.jbc.2022.101867.
[42] A. Leal-Egaña, et al., The size-speed-force relationship governs migratory cell response to tumorigenic factors, Mol. Biol. Cell 28 (12) (Jun. 2017) 1612–1621, https://doi.org/10.1091/mbc.E16-10-0694.
[43] C.M. Kraning-Rush, J.P. Califano, C.A. Reinhart-King, Cellular traction stresses increase with increasing metastatic potential, PLoS One 7 (2) (Feb. 2012) e32572, https://doi.org/10.1371/journal.pone.0032572.
[44] C.W. Molter, E.F. Muszynski, Y. Tao, T. Trivedi, A. Clouvel, A.J. Ehrlicher, Prostate cancer cells of increasing metastatic potential exhibit diverse contractile forces, cell stiffness, and motility in a microenvironment stiffness-dependent manner, Front. Cell Dev. Biol. 10 (Sep) (2022), https://doi.org/10.3389/fcell.2022.932510.
[45] B. Sabass, M.L. Gardel, C.M. Waterman, U.S. Schwarz, High resolution traction force microscopy based on experimental and computational advances, Biophys. J. 94 (1) (Jan. 2008) 207–220, https://doi.org/10.1529/biophysj.107.113670.
[46] G. Sarnighausen, et al., Traction force microscopy for linear and nonlinear elastic materials as a parameter identification inverse problem, Inverse Probl. 41 (6) (Jun. 2025) 065023, https://doi.org/10.1088/1361-6420/add0d5.
[47] A. Apolinar-Fernández, J. Barrasa-Fano, M. Cóndor, H. Van Oosterwyck, J. A. Sanz-Herrera, Traction force reconstruction assessment on real three-dimensional matrices and cellular morphologies, Int. J. Eng. Sci. 186 (May 2023), https://doi.org/10.1016/j.ijengsci.2023.103828.
[48] O.Y. Dudaryeva, S. Bernhard, M.W. Tibbitt, C. Labouesse, Implications of cellular mechanical memory in bioengineering, Am. Chem. Soc. (Nov. 13, 2023), https://doi.org/10.1021/acsbiomaterials.3c01007.
[49] P. Blázquez-Carmona, et al., Quantitative atlas of collagen hydrogels reveals mesenchymal cancer cell traction adaptation to the matrix nanoarchitecture, Acta Biomater. 185 (Sep. 2024) 281–295, https://doi.org/10.1016/j.actbio.2024.07.002.
[50] J. Steinwachs, et al., Three-dimensional force microscopy of cells in biopolymer networks, Nat. Methods 13 (2) (Feb. 2016) 171–176, https://doi.org/10.1038/nmeth.3685.
[51] Y. Zheng, M.B. Graeber, Microglia and Brain Macrophages as Drivers of Glioma Progression, MDPI, Dec. 01, 2022, https://doi.org/10.3390/ijms232415612.
[52] C.C. Poon, S. Sarkar, V.W. Yong, J.J.P. Kelly, Glioblastoma-Associated Microglia and Macrophages: Targets for Therapies to Improve Prognosis', Jun. 01, Oxford University Press, 2017, https://doi.org/10.1093/brain/aww355.
[53] T. Dudiki, et al., Microglia control vascular architecture via a TGFβ1 dependent paracrine mechanism linked to tissue mechanics, Nat. Commun. 11 (1) (Dec. 2020), https://doi.org/10.1038/s41467-020-14787-y.
[54] C. Dello Russo, et al., The human microglial HMC3 cell line: where do we stand? A systematic literature review, J. Neuroinflammation 15 (1) (2018) 259, https://doi.org/10.1186/s12974-018-1288-0.
[55] C. Loh, et al., Microglia and brain macrophages are differentially associated with tumor necrosis in glioblastoma: a link to tumor progression, Oncol. Res. 33 (4) (2025) 937–950, https://doi.org/10.32604/or.2024.056436.
[56] D. Matias, et al., Microglia/astrocytes–glioblastoma Crosstalk: Crucial Molecular Mechanisms and Microenvironmental Factors, Frontiers Media S.A, Aug. 03, 2018, https://doi.org/10.3389/fncel.2018.00235.
[57] W. Diao, et al., Behaviors of glioblastoma cells in in vitro microenvironments, Sci. Rep. 9 (1) (Dec. 2019), https://doi.org/10.1038/s41598-018-36347-7.
[58] https://www.atcc.org/products/crl-2611.
[59] L.N. Kiseleva, A.V. Kartashev, N.L. Vartanyan, A.A. Pinevich, M.P. Samoilovich, A172 and T98G cell lines characteristics, Cell Tissue Biol. 10 (5) (Sep. 2016) 341–348, https://doi.org/10.1134/S1990519X16050072.
[60] I.V. Kholodenko, A.Y. Lupatov, Y.S. Kim, R.Y. Saryglar, R.V. Kholodenko, K. N. Yarygin, Mesenchymal properties of glioma cell lines, Bull. Exp. Biol. Med. 178 (1) (Nov. 2024) 122–129, https://doi.org/10.1007/s10517-024-06294-7.
[61] Confirmation of publication and licensing rights-open access [Online]. Available: https://BioRender.com/kiwec8v, 2025.
[62] Z. Balion, et al., Comparison of microglial morphology and function in primary cerebellar cell cultures on collagen and collagen-mimetic hydrogels, Biomedicines 10 (5) (May 2022), https://doi.org/10.3390/biomedicines10051023.
[63] Confirmation of publication and licensing rights-open access [Online]. Available: https://BioRender.com/kr2wit7, 2025.
[64] J.R. Tse, A.J. Engler, Preparation of Hydrogel Substrates with Tunable Mechanical Properties, 2010, https://doi.org/10.1002/0471143030.cb1016s47.
[65] C.E. Kandow, P.C. Georges, P.A. Janmey, K.A. Beningo, Polyacrylamide Hydrogels for Cell Mechanics: Steps Toward Optimization and Alternative Uses, 2007, https://doi.org/10.1016/S0091-679X(07)83002-0.
[66] A.K. Denisin, B.L. Pruitt, Tuning the range of polyacrylamide gel stiffness for mechanobiology applications, Am. Chem. Soc. (Aug. 31, 2016), https://doi.org/10.1021/acsami.5b09344.
[67] S. Scott, et al., Dynamic and reversible tuning of hydrogel viscoelasticity by transient polymer interactions for controlling cell adhesion, Adv. Mater. 37 (12) (Mar. 2025), https://doi.org/10.1002/adma.202408616.
[68] N. Jiri, S. Michael, E. Philipp, Micromechanical properties of polyacrylamide hydrogels measured by spherical nanoindentation, in: Key Engineering Materials, Trans Tech Publications Ltd, 2014, pp. 121–124. https://dx.doi.org/10.4028/www.scientific.net/KEM.606.121.
[69] R. Subramani, et al., The influence of swelling on elastic properties of polyacrylamide hydrogels, Front Mater 7 (Jul) (2020), https://doi.org/10.3389/fmats.2020.00212.
[70] A.M. Smith, D.G. Inocencio, B.M. Pardi, A. Gopinath, R.C. Andresen Eguiluz, Facile determination of the poisson's ratio and young's modulus of polyacrylamide gels and polydimethylsiloxane, ACS Appl. Polym. Mater. 6 (4) (Feb. 2024) 2405–2416, https://doi.org/10.1021/acsapm.3c03154.
[71] J.L. Hay, P.J. Wolff, Small Correction Required when Applying the Hertzian Contact Model to Instrumented Indentation Data, ', 2001.
[72] D.C. Lin, D.I. Shreiber, E.K. Dimitriadis, F. Horkay, Spherical indentation of soft matter beyond the Hertzian regime: numerical and experimental validation of hyperelastic models, Biomech. Model. Mechanobiol. 8 (5) (2009) 345–358, https://doi.org/10.1007/s10237-008-0139-9.
[73] T. Boudou, J. Ohayon, C. Picart, R.I. Pettigrew, P. Tracqui, Nonlinear Elastic Properties of Polyacrylamide Gels: Implications for Quantification of Cellular Forces, IOS Press, 2009, https://doi.org/10.3233/BIR-2009-0540.
[74] G. Wu, M. Gotthardt, M. Gollasch, Assessment of nanoindentation in stiffness measurement of soft biomaterials: kidney, liver, spleen and uterus, Sci. Rep. 10 (1) (Dec. 2020), https://doi.org/10.1038/s41598-020-75738-7.
[75] S. Huth, S. Sindt, C. Selhuber-Unkel, Automated analysis of soft hydrogel microindentation: impact of various indentation parameters on the measurement of Young's modulus, PLoS One 14 (8) (Aug. 2019), https://doi.org/10.1371/journal.pone.0220281.
[76] D. Xu, M.L. Hernandez Miranda, N.D. Evans, B.G. Sengers, M. Browne, R.B. Cook, Depth profiling via nanoindentation for characterisation of the elastic modulus and hydraulic properties of thin hydrogel layers, J. Mech. Behav. Biomed. Mater. 148 (Dec) (2023), https://doi.org/10.1016/j.jmbbm.2023.106195.
[77] C. Li, J. Allen, T. Alliston, L.A. Pruitt, The use of polyacrylamide gels for mechanical calibration of cartilage - a combined nanoindentation and unconfined compression study, J. Mech. Behav. Biomed. Mater. 4 (7) (Oct. 2011) 1540–1547, https://doi.org/10.1016/j.jmbbm.2011.02.004.
[78] N.R. Richbourg, M.K. Rausch, N.A. Peppas, Cross-evaluation of stiffness measurement methods for hydrogels, Polymer (Guildf.) 258 (Oct. 2022), https://doi.org/10.1016/j.polymer.2022.125316.
[79] J.L. Martiel, et al., Measurement of cell traction forces with ImageJ, Methods Cell Biol. 125 (2015) 269–287, https://doi.org/10.1016/bs.mcb.2014.10.008.
[80] S. Huth, J.W. Blumberg, D. Probst, J. Lammerding, U.S. Schwarz, C. Selhuber-Unkel, Quantifying force transmission through fibroblasts: changes of traction forces under external shearing, Eur. Biophys. J. 51 (2) (2022) 157–169.

[81] C. Yang, M.W. Tibbitt, L. Basta, K.S. Anseth, Mechanical memory and dosing influence stem cell fate, Nat. Mater. 13 (6) (2014) 645–652, https://doi.org/10.1038/nmat3889.
[82] O. Habanjar, M. Diab-Assaf, F. Caldefie-Chezet, L. Delort, 3D Cell Culture Systems: Tumor Application, Advantages, and Disadvantages, MDPI, Nov. 01, 2021, https://doi.org/10.3390/ijms222212200.
[83] A.M. Burgoyne, et al., Proteolytic cleavage of protein tyrosine phosphatase μ regulates glioblastoma cell migration, Cancer Res. 69 (17) (Sep. 2009) 6960–6968, https://doi.org/10.1158/0008-5472.CAN-09-0863.
[84] M. Nakada, Y. Okada, J. Yamashita, THE ROLE OF MATRIX METALLOPROTEINASES IN GLIOMA INVASION, 2003.
[85] K. Wolf, P. Friedl, Extracellular Matrix Determinants of Proteolytic and Non-proteolytic Cell Migration, Dec. 2011, https://doi.org/10.1016/j.tcb.2011.09.006.
[86] A. Kwiatkowska, M. Kijewska, M. Lipko, U. Hibner, B. Kaminska, Downregulation of Akt and FAK phosphorylation reduces invasion of glioblastoma cells by impairment of MT1-MMP shuttling to lamellipodia and downregulates MMPs expression, Biochim. Biophys. Acta Mol. Cell Res. 1813 (5) (May 2011) 655–667, https://doi.org/10.1016/j.bbamcr.2011.01.020.
[87] H. Weidemann, D. Feger, J.E. Ehlert, M.M. Menger, R.C. Krempien, Markedly divergent effects of Ouabain on a temozolomide-resistant (T98G) vs. a temozolomide-sensitive (LN229) Glioblastoma cell line, Discov. Oncol. 14 (1) (Dec. 2023), https://doi.org/10.1007/s12672-023-00633-2.
[88] A.A. Pinevich, I.I. Bode, N.L. Vartanyan, L.N. Kiseleva, A.V. Kartashev, M. P. Samoilovich, Temozolomide-resistant human T2 and T98G glioblastoma cells, Cell Tissue Biol. 16 (4) (Aug. 2022) 339–351, https://doi.org/10.1134/S1990519X22040058.
[89] T. Andersen, et al., Cell size and actin architecture determine force generation in optogenetically activated cells, Biophys. J. 122 (4) (Feb. 2023) 684–696, https://doi.org/10.1016/j.bpj.2023.01.011.
[90] N. Nisenholz, et al., Active mechanics and dynamics of cell spreading on elastic substrates, Soft Matter 10 (37) (Oct. 2014) 7234–7246, https://doi.org/10.1039/c4sm00780h.
[91] S. Abuhattum, A. Gefen, D. Weihs, Ratio of total traction force to projected cell area is preserved in differentiating adipocytes, Integr. Biol. 7 (10) (Oct. 2015) 1212–1217, https://doi.org/10.1039/c5ib00056d.
[92] I. Dagogo-Jack, A.T. Shaw, Tumour Heterogeneity and Resistance to Cancer Therapies, Nature Publishing Group, Feb. 01, 2018, https://doi.org/10.1038/nrclinonc.2017.166.
[93] L. Bao, et al., The Relationship Between Cancer and Biomechanics, Frontiers Media SA, 2023, https://doi.org/10.3389/fonc.2023.1273154.
[94] A. Beliveau, G. Thomas, J. Gong, Q. Wen, A. Jain, Aligned nanotopography promotes a migratory state in glioblastoma multiforme tumor cells, Sci. Rep. 6 (May 2016), https://doi.org/10.1038/srep26143.
[95] R. Rezk, et al., Spatial heterogeneity of cell-matrix adhesive forces predicts human glioblastoma migration, Neurooncol. Adv. 2 (1) (Jan. 2020), https://doi.org/10.1093/noajnl/vdaa081.
[96] M.E. Oraiopoulou, et al., Integrating in vitro experiments with in silico approaches for Glioblastoma invasion: the role of cell-to-cell adhesion heterogeneity, Sci. Rep. 8 (1) (Dec. 2018), https://doi.org/10.1038/s41598-018-34521-5.
[97] S.J. Blaschke, et al., Substrate elasticity exerts functional effects on primary microglia, Front. Cell. Neurosci. 14 (Nov) (2020), https://doi.org/10.3389/fncel.2020.590500.
[98] L. Bollmann, et al., Microglia mechanics: immune activation alters traction forces and durotaxis, Front. Cell. Neurosci. 9 (September) (Sep. 2015) 1–16, https://doi.org/10.3389/fncel.2015.00363.
[99] M. Prinz, J. Priller, Microglia and Brain Macrophages in the Molecular Age: from Origin to Neuropsychiatric Disease, Nature Publishing Group, 2014, https://doi.org/10.1038/nrn3722.
[100] P. Melo, R. Socodato, M.S. Silveira, M.A.D. Neves, J.B. Relvas, I. Mendes Pinto, Mechanical actuators in microglia dynamics and function, Eur. J. Cell Biol. 101 (3) (Aug. 2022), https://doi.org/10.1016/j.ejcb.2022.151247.
[101] A.I. Bachir, A.R. Horwitz, W.J. Nelson, J.M. Bianchini, Actin-based adhesion modules mediate cell interactions with the extracellular matrix and neighboring cells, Cold Spring Harbor Perspect. Biol. 9 (7) (2017), https://doi.org/10.1101/cshperspect.a023234.
[102] D.W. Zhou, et al., Force-FAK signaling coupling at individual focal adhesions coordinates mechanosensing and microtissue repair, Nat. Commun. 12 (1) (Dec. 2021), https://doi.org/10.1038/s41467-021-22602-5.
[103] B. Geiger, J.P. Spatz, A.D. Bershadsky, Environmental Sensing Through Focal Adhesions, Jan. 2009, https://doi.org/10.1038/nrm2593.
[104] M. Ochsner, M. Textor, V. Vogel, M.L. Smith, Dimensionality controls cytoskeleton assembly and metabolism of fibroblast cells in response to rigidity and shape, PLoS One 5 (3) (2010), https://doi.org/10.1371/journal.pone.0009445.
[105] S.C. Bodine, et al., Taking cell-matrix adhesions to the third dimension, Science (1979) 294 (5547) (Nov. 2001) 1704–1708, https://doi.org/10.1126/science.1065874.
[106] Y. Zhang, et al., Run-and-Tumble dynamics and mechanotaxis discovered in microglial migration, Research 6 (Jan) (2023), https://doi.org/10.34133/research.0063.
[107] P.T. Nguyen, et al., Microglial remodeling of the extracellular matrix promotes synapse plasticity, Cell 182 (2) (Jul. 2020) 388–403.e15, https://doi.org/10.1016/j.cell.2020.05.050.
[108] H. Hamidi, J. Ivaska, Every step of the way: integrins in cancer progression and metastasis, Nature Res. (2018), https://doi.org/10.1038/s41568-018-0038-z.
[109] M. Nagano, D. Hoshino, N. Koshikawa, T. Akizawa, M. Seiki, Turnover of Focal Adhesions and Cancer Cell Migration, 2012, https://doi.org/10.1155/2012/310616.
[110] M.C. Brown, I. Staniszewska, P. Lazarovici, G.P. Tuszynski, L. Del Valle, C. Marcinkiewicz, Regulatory effect of nerve growth factor in α9β1 integrin-dependent progression of glioblastoma, Neuro Oncol. 10 (6) (2008) 968–980, https://doi.org/10.1215/15228517-2008-0047.
[111] M. Naumowicz, M. Kusaczuk, M. Zając, M. Gál, J. Kotyńska, Monitoring of the surface charge density changes of human glioblastoma cell membranes upon cinnamic and ferulic acids treatment, Int. J. Mol. Sci. 21 (18) (Sep. 2020) 1–15, https://doi.org/10.3390/ijms21186972.
[112] P.G. Gritsenko, P. Friedl, Adaptive adhesion systems mediate glioma cell invasion in complex environments, J. Cell Sci. 131 (15) (Aug. 2018), https://doi.org/10.1242/jcs.216382.
[113] T.A. Ulrich, E.M. De Juan Pardo, S. Kumar, The mechanical rigidity of the extracellular matrix regulates the structure, motility, and proliferation of glioma cells, Cancer Res. 69 (10) (May 2009) 4167–4174, https://doi.org/10.1158/0008-5472.CAN-08-4859.
[114] E.B. Oh, B. Meckes, J. Chang, D. Shin, C.A. Mirkin, Controlled glioma cell migration and confinement using biomimetic-patterned hydrogels, Adv. Nanobiomed. Res 2 (1) (Jan. 2022), https://doi.org/10.1002/anbr.202100131.
[115] I.E. Palamà, S. D'Amone, B. Cortese, Microenvironmental Rigidity of 3D Scaffolds and Influence on Glioblastoma Cells: a Biomaterial Design Perspective, Frontiers Media S.A, Sep. 24, 2018, https://doi.org/10.3389/fbioe.2018.00131.
[116] P. Sharma, K. Sheets, S. Elankumaran, A.S. Nain, The mechanistic influence of aligned nanofibers on cell shape, migration and blebbing dynamics of glioma cells, Integr. Biol. 5 (8) (Jul. 2013) 1036–1044, https://doi.org/10.1039/c3ib40073e.
[117] B.J. DuChez, A.D. Doyle, E.K. Dimitriadis, K.M. Yamada, Durotaxis by human cancer cells, Biophys. J. 116 (4) (Feb. 2019) 670–683, https://doi.org/10.1016/j.bpj.2019.01.009.
[118] K.B. Pointer, P.A. Clark, A.B. Schroeder, M.S. Salamat, K.W. Eliceiri, J.S. Kuo, Association of collagen architecture with glioblastoma patient survival, J. Neurosurg. 126 (6) (Jun. 2017) 1812–1821, https://doi.org/10.3171/2016.6.JNS152797.
[119] Confirmation of publication and licensing rights-open access [Online]. Available: https://BioRender.com/zcart2n, 2025.
[120] K. Molyneaux, et al., Physically-cross-linked poly(vinyl alcohol) cell culture plate coatings facilitate preservation of cell–cell interactions, spheroid formation, and stemness, J. Biomed. Mater. Res. B Appl. Biomater. 109 (11) (Nov. 2021) 1744–1753, https://doi.org/10.1002/jbm.b.34832.
[121] E. Mohiuddin, H. Wakimoto, Extracellular matrix in glioblastoma: opportunities for emerging therapeutic approaches [Online]. Available: www.ajcr.us/, 2021.
[122] M. Ravi, V. Paramesh, S.R. Kaviya, E. Anuradha, F.D. Paul Solomon, 3D cell culture systems: advantages and applications, J. Cell. Physiol. 230 (1) (Jan. 2015) 16–26, https://doi.org/10.1002/jcp.24683.
[123] V. Gkretsi, T. Stylianopoulos, Cell Adhesion and Matrix Stiffness: Coordinating Cancer Cell Invasion and Metastasis, Frontiers Media S.A, May 04, 2018, https://doi.org/10.3389/fonc.2018.00145.
[124] A. Acharekar, et al., Substrate stiffness regulates the recurrent glioblastoma cell morphology and aggressiveness: recurrent GBM have differential mechanosignaling response, Matrix Biol. 115 (Jan. 2023) 107–127, https://doi.org/10.1016/j.matbio.2022.12.002.
[125] S. Sinha, et al., Matrix stiffness regulates GBM migration and chemoradiotherapy responses via chromatin condensation in 3D viscoelastic matrices, ACS Appl. Mater. Interfaces (2025), https://doi.org/10.1021/acsami.4c16993.
[126] C. Cuni-Lopez, et al., 3D models of Alzheimer's disease patient microglia recapitulate disease phenotype and show differential drug responses compared to 2D, Jul 29 (2021), https://doi.org/10.21203/rs.3.rs-571254/v2.
[127] A. Marino, et al., Two-photon polymerization of sub-micrometric patterned surfaces: investigation of cell-substrate interactions and improved differentiation of neuron-like cells, ACS Appl. Mater. Interfaces 5 (24) (Dec. 2013) 13012–13021, https://doi.org/10.1021/am403895k.
[128] A. Bauer, M. Prechová, L. Fischer, I. Thievessen, M. Gregor, B. Fabry, pyTFM: a tool for traction force and monolayer stress microscopy, PLoS Comput. Biol. 17 (6) (Jun. 2021), https://doi.org/10.1371/journal.pcbi.1008364.
[129] A.B.C. Buskermolen, N.A. Kurniawan, C.V.C. Bouten, An automated quantitative analysis of cell, nucleus and focal adhesion morphology, PLoS One 13 (3) (Mar. 2018), https://doi.org/10.1371/journal.pone.0195201.
[130] J. Chen, Nanobiomechanics of Living Cells: a Review, Royal Society, Apr. 06, 2014, https://doi.org/10.1098/rsfs.2013.0055.
[131] N.Q. Balaban, et al., Force and focal adhesion assembly: a close relationship studied using elastic micropatterned substrates [Online]. Available: http://cellbio.nature.com466, 2001.
[132] M. Ghibaudo, et al., Traction forces and rigidity sensing regulate cell functions, Soft Matter 4 (9) (2008) 1836–1843, https://doi.org/10.1039/b804103b.
[133] J. Solon, I. Levental, K. Sengupta, P.C. Georges, P.A. Janmey, Fibroblast adaptation and stiffness matching to soft elastic substrates, Biophys. J. 93 (12) (Dec. 2007) 4453–4461, https://doi.org/10.1529/biophysj.106.101386.
[134] R.J. Pelham, Y.-L. Wang, Cell locomotion and focal adhesions are regulated by substrate flexibility [Online]. Available: www.pnas.org, 1997.
[135] K.A. Beningo, M. Dembo, I. Kaverina, J.V. Small, Y.-L. Wang, Nascent focal adhesions are responsible for the generation of strong propulsive forces in

migrating fibroblasts [Online]. Available: http://www.jcb.org/cgi/content/full/153/4/881, 2001.
[136] J. Stricker, Y. Aratyn-Schaus, P.W. Oakes, M.L. Gardel, Spatiotemporal constraints on the force-dependent growth of focal adhesions, Biophys. J. 100 (12) (2011) 2883–2893, https://doi.org/10.1016/j.bpj.2011.05.023.
[137] P.W. Oakes, Y. Beckham, J. Stricker, M.L. Gardel, Tension is required but not sufficient for focal adhesion maturation without a stress fiber template, JCB (J. Cell Biol.) 196 (3) (Feb. 2012) 363–374, https://doi.org/10.1083/jcb.201107042.
[138] P.W. Oakes, M.L. Gardel, Stressing the Limits of Focal Adhesion Mechanosensitivity, Elsevier Ltd., 2014, https://doi.org/10.1016/j.ceb.2014.06.003.
[139] J. Rheinlaender, et al., Cortical cell stiffness is independent of substrate mechanics, Nat. Mater. 19 (9) (Sep. 2020) 1019–1025, https://doi.org/10.1038/s41563-020-0684-x.
[140] M. Prager-Khoutorsky, et al., Fibroblast polarization is a matrix-rigidity-dependent process controlled by focal adhesion mechanosensing, Nat. Cell Biol. 13 (12) (Dec. 2011) 1457–1465, https://doi.org/10.1038/ncb2370.
[141] C. Vincent, T.A. Siddiqui, L.C. Schlichter, Podosomes in migrating microglia: components and matrix degradation [Online]. Available: http://www.jneuroinflammation.com/content/9/1/190, 2012.
[142] S. Hu, et al., Podosome rings generate forces that drive saltatory osteoclast migration, Mol. Biol. Cell 22 (17) (Sep. 2011) 3120–3126, https://doi.org/10.1091/mbc.E11-01-0086.
[143] H. Schürmann, et al., Analysis of monocyte cell tractions in 2.5D reveals mesoscale mechanics of podosomes during substrate-indenting cell protrusion, J. Cell Sci. 135 (10) (May 2022), https://doi.org/10.1242/jcs.259042.
[144] J. Rheinlaender, H. Wirbel, T.E. Schäffer, Spatial correlation of cell stiffness and traction forces in cancer cells measured with combined SICM and TFM, RSC Adv. 11 (23) (Apr. 2021) 13951–13956, https://doi.org/10.1039/d1ra01277k.
[145] S.I. Fraley, et al., A distinctive role for focal adhesion proteins in three-dimensional cell motility, Nat. Cell Biol. 12 (6) (Jun. 2010) 598–604, https://doi.org/10.1038/ncb2062.
[146] J.M. Maher, J.C. Markey, D. Ebert-May, The other half of the story: effect size analysis in quantitative research, CBE-Life Sci. Educ. 12 (3) (Sep. 2013) 345–351, https://doi.org/10.1187/cbe.13-04-0082.
[147] S. Aznavoorian, B.A. Moore, L. Donita Alexander-Lister, S.L. Hallit, L.J. Windsor, J.A. Engler, Membrane type I-Matrix metalloproteinase-mediated degradation of type I collagen by oral squamous cell carcinoma cells 1 [Online]. Available: http://aacrjournals.org/cancerres/article-pdf/61/16/6264/2487171/ch1601006264.pdf, 2001.
[148] A.D. Doyle, Generation of 3D collagen gels with controlled diverse architectures, Curr. Protoc. Cell Biol. 2016 (2016) 10.20.1–10.20.16, https://doi.org/10.1002/cpcb.9.
[149] Y. Antonelli, et al., When mechanical stress matters: generation of Polyploid giant cancer cells in tumor-like microcapsules, Adv. Funct. Mater. 34 (35) (Aug. 2024), https://doi.org/10.1002/adfm.202311139.
[150] F. Colombo, et al., Fluctuations of dry and total mass of cells exposed to different molecular weights of polyethylene glycol, Adv. Nanobiomed. Res (Jul. 2023), https://doi.org/10.1002/anbr.202200156.
[151] T. Spratte, et al., Increasing the efficiency of thermoresponsive actuation at the microscale by direct laser writing of pNIPAM, Adv. Mater. Technol. 8 (1) (Jan. 2023), https://doi.org/10.1002/admt.202200714.
[152] J.-Y. Bouguet, 'Pyramidal Implementation of the Lucas Kanade Feature Tracker Description of the Algorithm'.
[153] lucas_bruce_d_1981_1'.
[154] J. Hanke, D. Probst, A. Zemel, U.S. Schwarz, S. Köster, Dynamics of force generation by spreading platelets, Soft Matter 14 (31) (2018) 6571–6581, https://doi.org/10.1039/c8sm00895g.
[155] C.N. Holenstein, U. Silvan, J.G. Snedeker, High-resolution traction force microscopy on small focal adhesions-improved accuracy through optimal marker distribution and optical flow tracking, Sci. Rep. 7 (Feb) (2017), https://doi.org/10.1038/srep41633.
[156] A. Mortazavi, et al., Traction force microscopy with DNA FluoroCubes, Apr 15 (2024), https://doi.org/10.1101/2024.04.12.589182.
[157] J.P. Butler, I. Marija Tolic, B. Fabry, J.J. Fredberg, Traction fields, moments, and strain energy that cellsexert on their surroundings, Am. J. Physiol. Cell Physiol. 282 (2002) 595–605, https://doi.org/10.1152/ajpcell.00270.2001.-Adherent.
[158] U.S. Schwarz, N.Q. Balaban, D. Riveline, A. Bershadsky, B. Geiger, S.A. Safran, Calculation of forces at focal adhesions from elastic substrate data: the effect of localized force and the need for regularization, Biophys. J. 83 (3) (2002) 1380–1394, https://doi.org/10.1016/S0006-3495(02)73909-X.
[159] U. Horzum, B. Ozdil, D. Pesen-Okvur, Step-by-step quantitative analysis of focal adhesions, MethodsX 1 (1) (2014) 56–59, https://doi.org/10.1016/j.mex.2014.06.004.
[160] J. Schindelin, et al., Fiji: an open-source Platform for biological-image Analysis, Jul. 2012, https://doi.org/10.1038/nmeth.2019.
[161] M. Linkert, et al., Metadata Matters: Access to Image Data in the Real World, May 31, 2010, https://doi.org/10.1083/jcb.201004104.
[162] PAVONE USER MANUAL 2 optics11life, com', 2022 [Online]. Available: www.optics11life.comVISITINGADDRESS.
[163] P. Virtanen, et al., SciPy 1.0: fundamental algorithms for scientific computing in Python, Nat. Methods 17 (3) (Mar. 2020) 261–272, https://doi.org/10.1038/s41592-019-0686-2.
[164] C.R. Harris, et al., Array Programming with Numpy, Nature Research, Sep. 17, 2020, https://doi.org/10.1038/s41586-020-2649-2.
[165] T. pandas development team, Pandas-Dev/Pandas: Pandas, Sep. 2024, https://doi.org/10.5281/zenodo.13819579. Zenodo.
[166] W. Mckinney, Data Structures for Statistical Computing, Python', 2010.
[167] M. Waskom, Seaborn: statistical data visualization, J. Open Source Softw. 6 (60) (Apr. 2021) 3021, https://doi.org/10.21105/joss.03021.
[168] F. Charlier, et al., Statannotations, Nov. 2024, https://doi.org/10.5281/zenodo.14258156. Zenodo.